UNIVERZITA PALACKÉHO V OLOMOUCI

PŘÍRODOVĚDECKÁ FAKULTA

KATEDRA OPTIKY

DIPLOMOVÁ PRÁCE

Optická implementace kvantových operací pro kvantové zpracování informace s využitím provázaných fotonů: APLIKACE ELEKTRONICKÉ DOPŘEDNÉ VAZBY

Autor:	Bc. Martina Miková
Studijní program:	N1701 Fyzika
Studijní obor:	Optika a optoelektronika
Forma studia:	prezenční
Vedoucí práce:	Prof. RNDr. Miloslav Dušek, Dr.
Konzultant:	Mgr. Miroslav Ježek, Ph.D.
Termín odevzdání práce:	

Prohlášení:

Prohlašuji, že jsem diplomovou práci "Optická implementace kvantových operací pro kvantové zpracování informace s využitím provázaných fotonů – aplikace elektronické dopředné vazby" vypracovala sama, s využitím zdrojů uvedených v seznamu literatury a souhlasím s jejím použitím pro potřeby katedry, včetně libovolné formy prezentace.

V Olomouci, 2. května 2011

Poděkování:

Tímto bych ráda poděkovala vedoucímu diplomové práce Prof. RNDr. Miloslavu Duškovi, Dr. za veškerou pomoc, poskytnuté rady, konzultace a cenné připomínky při zpracování této práce. Dále Bc. Heleně Fikerové za cennou pomoc a spolupráci na společném projektu. Mgr. Miroslavu Ježkovi, Ph.D., Bc. Ivovi Strakovi, Mgr. Michalu Mičudovi a Mgr. Lucii Čelechovské za rady, nápady a věnovaný čas, jak v oblasti teoretické, tak zejména experimentální. V neposlední řadě bych ráda poděkovala mojí rodině za podporu v průběhu celého studia.

Bibliografická identifikace:

Jméno a příjmení autora:	Bc. Martina Miková
Název práce:	Optická implementace kvantových operací pro kvantové zpracování informace s využitím provázaných fotonů - aplikace elektronické dopředné vazby
Typ práce:	Diplomová
Pracoviště:	Katedra optiky
Vedoucí práce:	Prof. RNDr. Miloslav Dušek, Dr.
Rok obhajoby práce:	2011
Počet stran:	52
Počet příloh:	0
Jazyk:	anglický

Klíčová slova:

kvantové programovatelné fázové hradlo, kvantový přenos informace, elektronická dopředná vazba, vláknová optika, Machův-Zehnderův interferometr

Abstrakt:

Cílem této práce je experimentální realizace kvantového programovatelného fázového hradla, které pootočí libovolný kvantový stav datové qubitu okolo osy z Blochovy sféry. Úhel rotace je zakódován ve stavu programového qubitu [1]. Hradlo je tvořeno dvěma vzájemně propojenými vláknovými Machovými-Zehnderovými interferometry, které pracují na jednofotonové úrovni. Informace je kódována do prostorových módů světla. Pomocí dopředné elektronické vazby jsme zvýšili pravděpodobnost úspěchu hradla na její teoretický limit.

PALACKY UNIVERSITY IN OLOMOUC

FACULTY OF SCIENCE

DEPARTMENT OF OPTICS

DIPLOMA THESIS

Optical implementation of quantum operation for quantum information processing using entangled photons: APLICATION OF ELECTRONIC FEED-FORWARD

Author:	Bc. Martina Miková
Study programm:	N1701 Physics
Field of Study:	Optics and optoelektronics
Form of study:	Full-time
Thesis Supervisor:	Prof. RNDr. Miloslav Dušek, Dr.
Thesis Co-Supervisor:	Mgr. Miroslav Ježek, Ph.D.
Date:	

Declaration:

I declare, that I elaborated my diploma thesis "Optical implementation of quantum operation for quantum information processing using entangled photons - application of electronic feed-forward" myself, using the resources listed in the references. I agree with its use for needs of the department, including an arbitrary form of presentation.

In Olomouc, 2^{nd} May 2011

Acknowledgement:

I would like to thank my thesis supervisor Prof. Miloslav Dušek, Dr. for all his help, advice, consultation and valuable comments he provided during elaboration of this thesis. Furthermore, I would also like to thank Bc. Helena Fikerová for her valuable assistance and cooperation in our joint project. Mgr. Miroslav Ježek, Ph.D., Bc. Ivo Straka , Mgr. Michal Mičuda and Mgr. Lucie Čelechovká for their advice, ideas and time boh in theoretical and especially experimental part. I would also like to thank my family for their support throughout the entire period of my studies.

Bibliographical identification:

Autor's first name and surname:	Bc. Martina Miková
Title:	Optical implementation of quantum operation for quantum information processing using entangled photons - application of electronic feed-forward
Type of thesis:	Diploma
Department:	Department of Optics
Supervisor:	Prof. RNDr. Miloslav Dušek, Dr.
Year of presentation:	2011
Number of pages:	52
Number of appendices:	0
Language:	English

Keywords:

quantum programmable phase gate, quantum information processing, electronic feed-forward, fiber optics, Mach-Zender interferometer

Abstract:

The aim of this thesis is the experimental implementation of a quantum programmable phase gate. This gate rotates an arbitrary quantum state of the data qubit around the z-axis of the Bloch sphere. The angle of rotation is encoded into the program qubit state [1]. The gate consists of two interconnected fibre Mach-Zender interferometers operating at a single photon level. Information is encoded into spatial modes of light. We use electronic feed-forward to increase the success probability of the gate to its theoretical limit.

Contents

1 Introduction

The aim of this diploma thesis is to propose, experimentally implement and test a quantum programmable phase gate. The use of electronic feed-forward enables us to correct improper results in linear-optical quantum gate in real time. Thus, we increase the success probability of the programmable phase gate from 25% (already reached in [2]) to its theoretical limit of 50% [1]. The feed-forward principle itself was tested last year [12].

Our quantum programmable phase gate is implemented using fibre optics components. Information is encoded into spatial modes of light. The core of the gate is represented by two interconnected fibre Mach-Zehnder interferometers operating at a single photon level. We use time-correlated pairs of photons generated by frequency parametric down conversion. Signal and idler photons represent data and program qubits, respectively.

The programmable phase gate rotates an arbitrary quantum state of the data qubit around the z-axis of the Bloch sphere by angle φ. The angle of rotation, i.e. a phase shift, is encoded into the state of the program qubit [1]. The feed-forward enables us to affect the output state of the data qubit according to the result of measurement on the program qubit. Incorrect output states of the data qubit are changed to the required ones. In this way the theoretical limit of the success probability is reached.

The thesis starts with the discussion why is it interesting to pay attention to quantum information processing. Then we summarize essential results and testing methods concerning the electronic feed-forward [12]. The next chapters are devoted to the experiment, especially to its preparation, construction, alignment and control. Then we deal with software for controlling the experiment through PC. Namely, we describe programs for controling phase modulators, variable ratio splitters and other devices. Then we describe how to align individual components and the entire device. We also describe the source of time-correlated photons and its sophisticated integration with a probe laser diode. Further, we discuss how to ensure a maximum stability of the experiment by means of passive and active methods. We explain the idea of the program for active stabilization of the both interconnected interferometers at the same time using phase modulators. Next we discuss the main program which sets, step by step, the input states of the gate as well as the all measurement basis for tomography measurement. In fact, it links together particular subroutines already mentioned. Next we deal with the data processing of measurement results. Finally, we summarize the results of the first tests of the programmable phase gate with

and without feed-forward.

2 Motivation

Current information technology exploits classical physics for processing and storage of information. However, we still need new methods and algorithms for solving problems, because computing capacity of classical computers is largely limited and many classical alghoritms are inefficient, and we want yet smaller, faster and more powerful computers. Quantum information processing uses quantum mechanics for manipulating information. It enables us to solve some of the problems faster and more efficiently, e.g. factorization of large number, search in unsorted database etc. The computing time of the all known classical algorithms for factorization of large numbers grows exponentialy with the length of the number.

But there is a quantum algorithm, known as Shor's factorization algorithm [6], whose computing time grows only with polynomial dependence. Classical algorithms for search in unsorted database with N elements need on average $N/2$ steps but quantum Grover's search algorihtm [7] needs only $\sqrt{N}$ steps with condition, that the database is encoded into a specific quantum state.

An elementary unit of classical information is a bit; it can take values 0 or 1 which represent some well defined levels of certain physical quantity, like voltage. A basic unit of quantum information is a quantum bit (qubit). Its state can be an arbitrary linear superposition of two basis states, $|\psi\rangle = \alpha|0\rangle + \beta|1\rangle$, where α and β are complex numbers, which represent amplitudes of probability. The basis states $|0\rangle$ and $|1\rangle$ are supposed to be orthonormal to each other, $\langle 0|1\rangle = 0$, $\langle 0|0\rangle = \langle 1|1\rangle = 1$, and span a two-dimensional Hilbert space. A qubit can be found in one of the basis states, $|0\rangle$ or $|1\rangle$, with probability of $|\alpha|^2$ and $|\beta|^2$, respectively (the probabilities must satisfy the normalization condition $|\alpha|^2 + |\beta|^2 = 1$).

To be able to do logical operations with classical bits, we need classical gates out of them we can build a whole classical processor which obeys laws of classical physics. If we want to build a quantum computer one day, we need a quantum logical gates as a basic building blocks of the future quantum processor. Quantum gate is a device which implements a unitary operation on qubits. There are quantum gates which are analogous to classical gates, but they can work with quantum superposition. On the other hand there is a group of quantum gates which have no

classical analogy.

In analogy to a register in classical computers – n qubits, which are ordered, create n-qubit quantum register. General state of the register is a superposition of 2^n basis states. Quantum register is thus described as a complex vector in 2^n dimensional Hilbert space. The dimension of Hilbert space grows exponentialy with the length of the register. Hilbert space of a quantum register is composed of a direct product of Hilbert spaces of single qubits. The most interesting feature of quantum register is that the constituent qubits can form an entangled state. Number of parameters which characterize a classical system grows only linearly with the length of the register. In some cases, it could give an exponential advantage to quantum systems. However, we cannot get complete information contained in quantum register only by single quantum measurement.

In our experiment, qubits are carried by photons. To be able to do some operations with photons in a logical gate, it is necessary to provide their interaction with each other in a controlled way (but they must not interact with the environment). To arrange such interaction is not so easy, they do not interact with each other very well. Their interaction can be mediated by nonlinear effects in material media, but it is difficult because at a single photon level the nonlinear effects are really weak. Fortunately, there is another possibility which is experimentally feasible. It uses linear optical components and quantum measurement. Because quantum measurement is non-linear (it breaks superpositions) it can substitute the nonlinearity of the system. By measuring on an auxiliary system the state of the whole system is changed. Unfortunately, quantum measurement is probabilistic – i.e., it gives random results – thus all linear-optics quantum gates are probabilistic too. It means they sometimes fail. Some increase of the success probability of linear optical gates can be achieved by the feed-forward technique (it will be discussed later). More details can be found in [17, 12, 16].

3 Theory

3.1 Encoding information

In quantum communication and quantum information processing information is also encoded into physical systems. Any two-level (or multi-level) physical system can be used as a qubit. As we stated, we use photons as qubits in our experiment. We can encode information into light thanks to its well defined physical properties such as: polarization, photon number, spatial and

temporal modes, angular momentum, etc. In the polarization encoding of information, the two well distinguishable basis states can be defined e.g. horizontal and vertical linear polarizations of light, right and left circular polarizations of light, etc. Encoding using photon number has basis states with arbitrary, but well defined, numbers of photons. E.g. with and without photon, i.e. single photon state and vacuum state, or one and two photons, etc. We can also discriminate time of photon arrival, it is called time-bin encoding and the two basis states are represented by earlier and later arrivals of the photon. Encoding of information into spatial modes uses the basis states which are represented by the passage of the photon through one or another path. It should be noted that one or more qubits can be encoded into one photon. In our experiment we exploit encoding of information into spatial modes of light.

3.2 Beam splitter (BS)

Beam splitter is an optical device which divides an optical beam into two parts. It has two inputs and two outputs, see Fig. 3.1a. An important characteristic of the BS is its splitting ratio.

For lossless beam splitter it applies: $|r|^2 + |t|^2 = |r'|^2 + |t'|^2 = 1$, and $rt^* + r'^*t' = 0$, where r, r', t, t' are reflectances and transmittances (they are in general complex numbers), see Fig. 3.1a, and the asterisk denotes complex conjugation. The phase shift of the transmission and reflection must fulfill the following condition: $\arg(r)+\arg(r')-\arg(t)-\arg(t') = (1-2k)\pi$. It was deduced from energy conservation law by G. G. Stokes [9],see also [10, 11]. The creation operators of the input modes 1, 2 of the BS (a_1^+, a_2^+) can be expressed using the creation operators of output modes 3, 4 of the BS (a_3^+, a_4^+) and vice versa [17]. The relations describing the BS using creation operators (a^+) read

$$\begin{aligned} a_1^+ &= ra_3^+ + ta_4^+, \\ a_2^+ &= t'a_3^+ + r'a_4^+, \qquad (3.1) \\ a_3^+ &= r^*a_1^+ + t'^*a_2^+, \\ a_4^+ &= t^*a_1^+ + r'^*a_2^+. \qquad (3.2) \end{aligned}$$

In the following text we will suppose, without the loss of generality, that reflection imposes the phase shift of $\pi/2$. The value of the phase shift is arbitrary, but it has to satisfy the Stokes relations. When the splitting ratio of the BS is 50:50, $r = r' = \frac{i}{\sqrt{2}}$ and $t = t' = \frac{1}{\sqrt{2}}$, thus

$|t| = |r|$, the relations for creation operators read

$$\begin{aligned} a_1^+ &= \frac{1}{\sqrt{2}}\left(i\, a_3^+ + a_4^+\right), \\ a_2^+ &= \frac{1}{\sqrt{2}}\left(a_3^+ + i\, a_4^+\right), \qquad (3.3) \\ a_3^+ &= \frac{1}{\sqrt{2}}\left(-i\, a_1^+ + a_2^+\right), \\ a_4^+ &= \frac{1}{\sqrt{2}}\left(a_1^+ + -i\, a_2^+\right). \qquad (3.4) \end{aligned}$$

The previous transformation rules hold for both horizontal and vertical polarization modes, thus it is polarization insensitive beam-splitter.

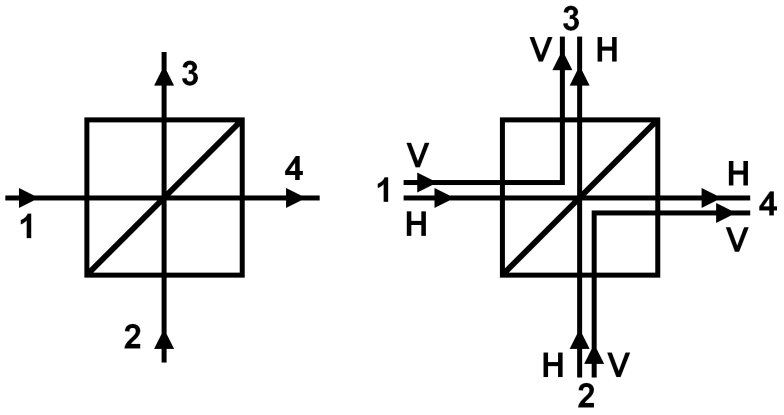

(a) Beam splitter (BS) (b) Polarizing beam splitter(PBS)

Figure 3.1: Scheme of BS and PBS, 1, 2 – input modes, 3, 4 – output modes, V – vertical polarization, H – horizontal polarization

3.3 Polarizing beam splitter (PBS)

The polarizing beam splitter is a special type of beam splitter, which totally reflects vertically polarized photons (V) and transmits horizontally polarized photons (H). Thus $t_V = t'_V = r_H = r'_H = 0$, $r_V = r'_V = 1 \cdot e^{i\pi/2} = i$, $t_H = t'_H = 1$, see Fig. 3.1b. Transformations of creation operators (a^+) by PBS read

for vertical polarization:

$$a_{V1}^{+} = ia_{V3}^{+}, \qquad a_{V2}^{+} = ia_{V4}^{+}, \tag{3.5}$$

for horizontal polarization:

$$a_{H1}^{+} = a_{H4}^{+}, \qquad a_{H2}^{+} = a_{H3}^{+}. \tag{3.6}$$

3.4 Classical description of Mach-Zehnder (MZ) interferometer

The Mach-Zehnder interferometer is one of the basic interferometric devices. It consists of two beam splitters, two mirrors (M) and two detectors (when we consider a bulk-optics setup). Let us suppose that the beam-splitters have 50:50 splitting ratios and impose the phase shifts of $\pi/2$ into the reflected parts of the beams and zero phase shifts into transmitted parts of the beams. The mirrors have reflectivity of 100% and we suppose they do not introduce any aditional phase shifts [1] [17, 12].

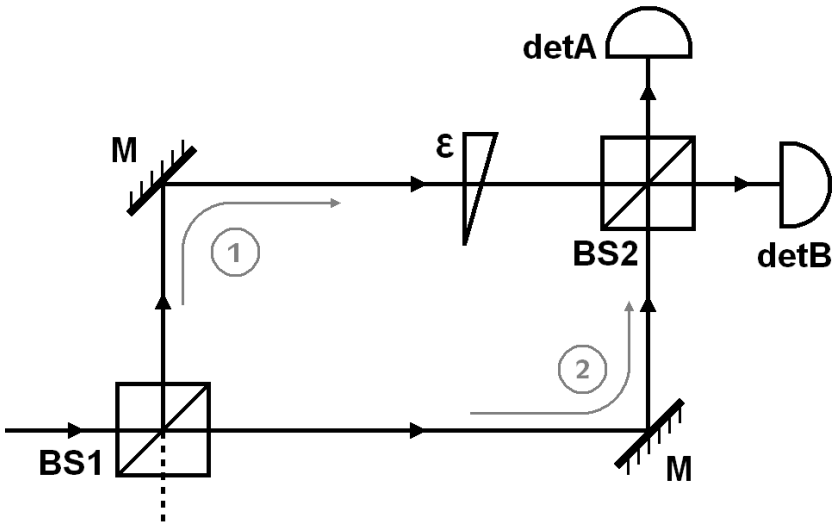

Figure 3.2: The Mach-Zehnder interferometer with incoming light from the left side; BS1, BS2 – beam-splitters, M_1,M_2 – mirrors, detA, detB – detectors, ϵ – general phase shift between the intereferometer arms

The input light beam enters the first beam-splitter (BS1) and is split to two arms 1, 2 of the interferometer. Then the both beams are reflected by mirrors (M_1,M_2), see Fig. (3.2). Generally,

[1] But be careful, for different polarization components the mirrors impose different phase shifts.

there can be another phase shift ϵ between the two interferometer arms due to the difference of their lengths,

$$\epsilon = \frac{2\pi}{\lambda} \cdot d = \frac{2\pi}{\lambda} \cdot c \cdot \tau, \tag{3.7}$$

where d is the difference between optical paths of arms 1 and 2, c is the speed of light in the media and τ is the time delay corresponding to optical path difference d.

Finally, the beams are combined again in the second beam splitter (BS2). The beams exiting BS2 through output A are phase shifted to each other by $\delta_A = \pi + \epsilon$. Analogicaly the beams exiting BS2 through output B are phase shifted to each other by $\delta_B = \epsilon$. If $\epsilon = \pi$ they interfere destructively and there is no signal at the detector A, at the moment the dector B detect maximum posible signal, because the beams interfere constructively and vice versa. By changing the phase difference $\epsilon = \epsilon(\tau)$ between interferometer arms we can observe interference fringes at detectors A and B. The value of the detected intensity is given by the interference law. Detectors A and B detect intensities I_A and I_B of incoming light, respectively [16]

$$I_A(t) = I_1 + I_2 + 2\sqrt{I_1 I_2} \cdot \cos(\epsilon) \cdot |\gamma_{12}(\tau)|,$$

$$I_B(t) = I_1 + I_2 + 2\sqrt{I_1 I_2} \cdot \cos(\epsilon + \pi) \cdot |\gamma_{12}(\tau)| = I_1 + I_2 + 2\sqrt{I_1 I_2} \cdot \sin(\epsilon) \cdot |\gamma_{12}(\tau)|.$$

Here I_1 and I_2 are intensities of the light beams passing through arms 1 and 2, respectively. Corresponding field amplitudes will be denoted u_1 and u_2. Complex degree of time correlation $\gamma_{12}(\tau)$ characterizes coherence between field amplitudes $u_1(t+\tau)$ and $u_2(t)$, $0 \leq |\gamma_{12}(\tau)| \leq 1$. The value of maximum intensity at the detector A and B is the same, $I_{A,max} = I_{B,max} = I_{max}$, the same is true for minimum intensity $I_{A,min} = I_{B,min} = I_{min}$, where

$$I_{min} = I_1 + I_2 - 2\sqrt{I_1 I_2} \cdot |\gamma_{12}(\tau)|, \tag{3.8}$$

$$I_{max} = I_1 + I_2 + 2\sqrt{I_1 I_2} \cdot |\gamma_{12}(\tau)|. \tag{3.9}$$

Visibility of interference fringes is a convenient parameter to quantify the quality of interference. It depends on the maximum and minimum intensities of the interference pattern,

$$V = \frac{I_{max} - I_{min}}{I_{max} + I_{min}} = 2 \cdot \frac{\sqrt{I_1 I_2}}{(I_1 + I_2)} \cdot |\gamma_{12}(\tau)|. \tag{3.10}$$

If the intensities in the both arms are equal, $I_1 = I_2$, then the visibility is fully characterized by the magnitude of the complex degree of time coherence, $V = |\gamma_{12}(\tau)|$. The complex degree of

time coherence $\gamma(\tau)$ is defined as a normalized autocorrelation function

$$\gamma(\tau) = \frac{\Gamma(\tau)}{\Gamma(0)} = \frac{\langle u(t+\tau) \cdot u^*(t) \rangle}{\left\langle |u(t)|^2 \right\rangle} \tag{3.11}$$

of the light source used. $\Gamma(0) = \left\langle |u(t)|^2 \right\rangle = I$ for $\tau = 0$. Thus $|\gamma_{12}(0)| = 1$ and the fringes visibility is 100%. When time delay τ is longer than the coherence time τ_c of radiation, $|\gamma_{12}(0)| \approx 0$ [16]. In this case the visibility is equal to 0.

But in the real life the fringe visibility of the MZ interferometer is usually lower than 100%. It is because of the BS imperfections and unequal losses in the arms [5]. By imperfections we mean that the splitting ratio of real BS is not exactly 50:50 and it is also sensitive on wave length. This affects the visibility. As will be shown, we can partially compensate these BS imperfections by extra losses in the arms. Of course, it is necessary to take into account already existing losses. In bulk MZ interferometer the losses are caused mainly by imperfect anti-reflex coating of the beam splitters and reflex coating of the mirrors. In fibre optical MZ interferometer the losses are caused by fibre connections and by other added components like phase modulators, air gaps, etc. (it will be discussed later). Beside there is absorption and scattering in material media [16, 5]. The visibility is also affected by spatial and polarization modes overlap. In fibres there is spatial mode overlap provided automatically.

3.5 Full quantum mechanical description of the MZ interf.

Now we describe the relations between creation operators of input and output modes of MZ interferometer. First we describe the lossless MZ interferometer using Eqs. (3.1) in their matrix form. The reflectances and transmittances of BS1 are denoted r_1, r_1', t_1, t_1' and similarly for BS2,

$$\begin{pmatrix} a_3^+ \\ a_4^+ \end{pmatrix} = \overbrace{\begin{pmatrix} r_2^* & t_2'^* \\ t_2^* & r_2'^* \end{pmatrix}}^{\text{BS2}} \cdot \overbrace{\begin{pmatrix} e^{i\epsilon} & 0 \\ 0 & 1 \end{pmatrix}}^{\text{free propagation}} \cdot \overbrace{\begin{pmatrix} r_1^* & t_1'^* \\ t_1^* & r_1'^* \end{pmatrix}}^{\text{BS1}} \cdot \begin{pmatrix} a_1^+ \\ a_2^+ \end{pmatrix},$$

$$\begin{pmatrix} a_3^+ \\ a_4^+ \end{pmatrix} = \begin{pmatrix} r_2^*\, r_1^*\, e^{i\epsilon} + t_1^*\, t_2'^* & r_2^*\, t_1'^*\, e^{i\epsilon} + r_1'^*\, t_2'^* \\ t_2^*\, r_1^*\, e^{i\epsilon} + t_1^*\, r_2'^* & t_2^*\, t_1'^*\, e^{i\epsilon} + r_1'^*\, r_2'^* \end{pmatrix} \cdot \begin{pmatrix} a_1^+ \\ a_2^+ \end{pmatrix}.$$

If the both beam-splitters have their splitting ratio equal to 50:50, the transformation simplifies to

$$\begin{pmatrix} a_3^+ \\ a_4^+ \end{pmatrix} = \frac{1}{2} \cdot \begin{pmatrix} -e^{i\epsilon} + 1 & -i\, e^{i\epsilon} - i \\ -ie^{i\epsilon} - i & e^{i\epsilon} - 1 \end{pmatrix} \cdot \begin{pmatrix} a_1^+ \\ a_2^+ \end{pmatrix}.$$

For example, if one photon enters the interferometr in input mode 1, see Fig. 3.2, i.e. the input state reads $a_1^+ |vac\rangle$, with $|vac\rangle$ beeing a vacuum state, then the output quantum state of light is $((-e^{i\epsilon}+1)a_3^+ + (-ie^{i\epsilon} - i)a_4^+)\,|vac\rangle$. The photon is detected by the detector A with probability $|-e^{i\epsilon}+1|^2$ and with probability $|-ie^{i\epsilon} - i|^2$ by the detector B. For phase shift $\epsilon = 0$ the photon is detected by the detector B with certainty.

Now we describe behaviour of a real MZ interferometer, i.e. MZ interferometer with imperfect beam-splitters and with non-zero losses in its arms. For purpose of this model we can represent these loses by additional beam-splitters BS3 and BS4 in each arm of the interferometer with reflectances and transmittances r_3, r_3', t_3, t_3' and r_4, r_4', t_4, t_4', respectively [5], see Fig. (3.3). We suppose that the phase shifts imposed by BS3 and BS4 are the same. A description with four

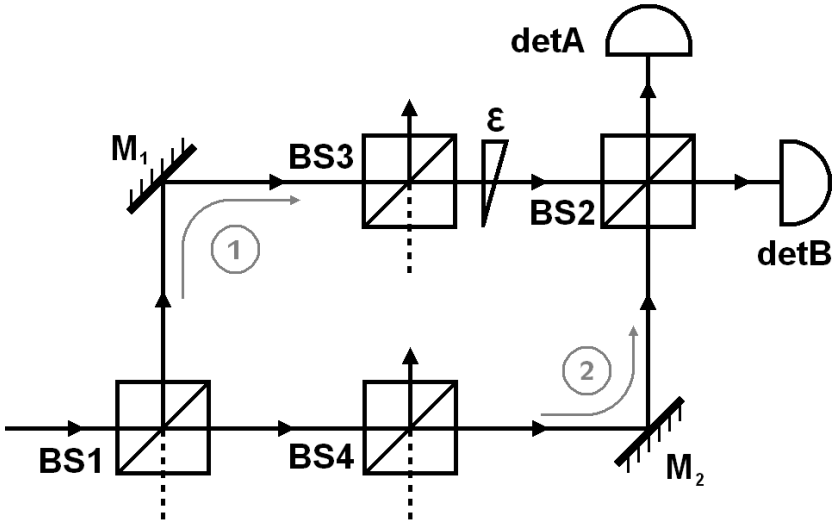

Figure 3.3: Model of a real Mach-Zehnder interferometer with light incoming from the left; BS1 and BS2 – input and output beam-splitters, BS3 and BS4 – added losses, M_1,M_2 – mirrors, detA, detB – detectors, ϵ – general phase shift between interferometer's arms

input and four output modes should by used for the presented model. But if there is a vacuum

in the second input mode of BS3 as well as BS4 we can simplify the description significantly,

$$\begin{pmatrix} a_3^+ \\ a_4^+ \end{pmatrix} = \overbrace{\begin{pmatrix} r_2^* & t_2'^* \\ t_2^* & r_2'^* \end{pmatrix}}^{\text{BS2}} \cdot \overbrace{\begin{pmatrix} e^{i\epsilon} & 0 \\ 0 & 1 \end{pmatrix}}^{\text{free propagation}} \cdot \overbrace{\begin{pmatrix} t_3^* & 0 \\ 0 & t_4^* \end{pmatrix}}^{\text{losses}} \cdot \overbrace{\begin{pmatrix} r_1^* & t_1'^* \\ t_1^* & r_1'^* \end{pmatrix}}^{\text{BS1}} \cdot \begin{pmatrix} a_1^+ \\ a_2^+ \end{pmatrix},$$

$$\begin{pmatrix} a_3^+ \\ a_4^+ \end{pmatrix} = \begin{pmatrix} r_2^*\, r_1^*\, e^{i\epsilon}\, t_3^* + t_1^*\, t_2'^*\, t_4^* & r_2^*\, t_1'^*\, e^{i\epsilon}\, t_3^* + r_1'^*\, t_2'^*\, t_4^* \\ t_2^*\, r_1^*\, e^{i\epsilon}\, t_3^* + t_1^*\, r_2'^*\, t_4^* & t_2^*\, t_1'^*\, e^{i\epsilon}\, t_3^* + r_1'^*\, r_2'^*\, t_4^* \end{pmatrix} \cdot \begin{pmatrix} a_1^+ \\ a_2^+ \end{pmatrix}.$$

In the following part of the description we restrict to the case when the photons enter the BS1 only through the input 1.

To calculate a fringe visibility at detectors A and B we have to determine the corresponding rate of photodetection, I_A, I_B, as funtions of phase ϵ,

$$\begin{aligned} I_A(\epsilon) &\approx \left\langle a_3^+ a_3 \right\rangle = |r_2|^2|r_1|^2|t_3|^2 + |t_1|^2|t_2'|^2|t_4|^2 + 2|r_2||r_1||t_3||t_1||t_2'||t_4|\cos(\epsilon), \\ I_B(\epsilon) &\approx \left\langle a_3^+ a_3 \right\rangle = |t_2|^2|r_1|^2|t_3|^2 + |t_1|^2|r_2'|^2|t_4|^2 + 2|t_2||r_1||t_3||t_1||r_2'||t_4|\sin(\epsilon). \end{aligned} \quad (3.12)$$

The fringes visibilities at outputs A, B are given by relations Eq.(3.10) and Eqs.(3.12):

$$V_A = \frac{I_{Amax} - I_{Amin}}{I_{Amax} + I_{Amin}} = 2\left(\frac{|r_2||r_1||t_3|}{|t_1||t_2'||t_4|} + \frac{|t_1||t_2||t_4|}{|r_2||r_1||t_3|}\right)^{-1}, \quad (3.13)$$

$$V_B = \frac{I_{Bmax} - I_{Bmin}}{I_{Bmax} + I_{Bmin}} = 2\left(\frac{|t_2||r_1||t_3|}{|t_1||r_2'||t_4|} + \frac{|t_1||r_2'||t_4|}{|t_2||r_1||t_3|}\right)^{-1}. \quad (3.14)$$

If BS2 has an ideal 50:50 splitting ratio, it is possible to reach unity visibility at the both output ports of BS2, $V_A = V_B = 1$. The imperfections of BS1 can be compensated by additional losses in the arms. The conditions for obtaining unity visibilities at the both outputs read

$$|r_2| = \frac{1}{\sqrt{2}}, \qquad \frac{|r_1||t_3|}{|t_1||t_4|} = 1, \quad (3.15)$$

where $\frac{|t_3|}{|t_4|}$ is the ratio of losses in arms 1 and 2. If only one of these two conditions is fulfilled, visibilities at the both outputs are lower than one $V_A = V_B \neq 1$, but they are equal. Unfortunately, imperfections of BS2 cannot be fully compensated. But we can reach the unity visibility at least at one output port. To better understand this problem, we graphically illustrate the dependence of visibilities V_A, V_B on splitting ratio of BS1 and BS2, when loss ratio $\frac{|t_3|}{|t_4|}$ is equal to one, see

Fig. 3.4.

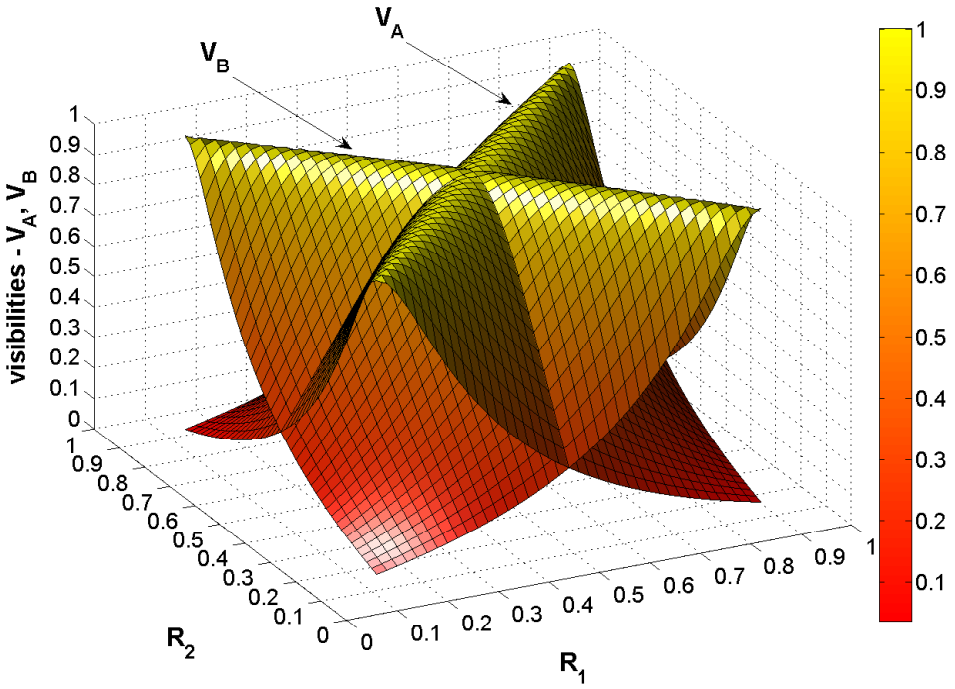

Figure 3.4: Dependence of fringes visibilities V_A, V_B on splitting ratios of BS1, BS2, where $R_1 = |r_1|^2$ and $R_2 = |r_2|^2$ and $\frac{|t_3|}{|t_4|} = 1$

3.6 Programmable quantum gates

At the beginning there was an idea of a universal quantum processing unity, where the state of program qubits determines the unitary transformation on data qubits [3]. Vidal, Manes, and Cirac proposed a basic programmable quantum gate [1]. They showed that a unitary operation cannot be, in general, deterministicaly encoded into a finite number of qubits. But it can be done probabilisticaly. Their scheme has failure probability 2^{-N}, where N is number of qubits in quantum program register. They proved that the maximum possible probability of success for a single-qubit program register is 50%.

They also suggested a programmable single-qubit gate, which rotates an arbitrary quantum state of the data qubit around the z-axis of the Bloch sphere, i.e. a quantum programmable phase gate. The angle of rotation φ (a phase shift) of the data qubit is encoded into the state of the program qubit [1, 2].

3.6.1 Programmable phase gate

The first, but non-optimal, implementation of the single-qubit programmable gate was built by M. Mičuda et al. [2]. Their bulk optical implementation was based on encoding of qubit states into the polarization modes of light. They exploited interference of two photons on a polarization beam-splitter (PBS), thus interference of the program and the data qubit. They implemented a passive version of the gate, without using any technique for correcting incorrect output state. Therefore the success probability of the gate was only 25%. The states are marked like $|V\rangle$ – one photon with vertical polarization and $|H\rangle$ – one photon with horizontal polarization.

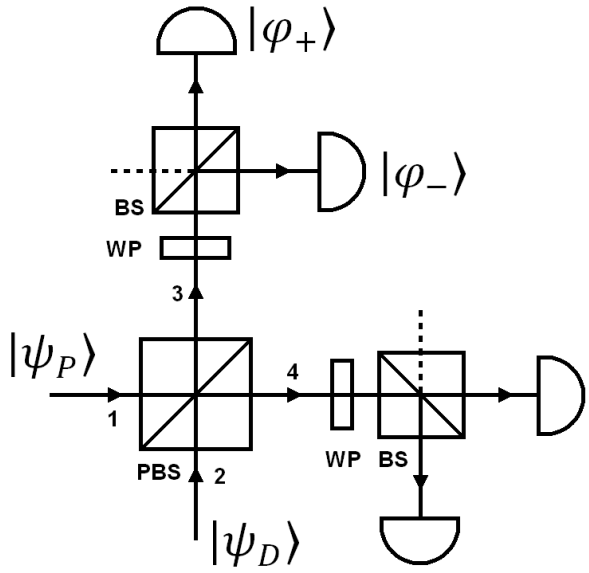

Figure 3.5: Scheme of the linear-optical programmable phase gate, using bulk components, PBS –polarizing beam splitter, BS – beam splitter, WP - wave plates

The program qubit in state $|\psi_P\rangle$ enters through the first input of PBS. It is prepared as an equal superposition of two basis states with a phase factor which carries the information about the angle of rotation φ. The data qubit in state $|\psi_D\rangle$ enters through the second input of PBS, its state is described as a general superposition of the two basis states

$$|\psi_P\rangle = \frac{1}{\sqrt{2}}(|V_1\rangle + e^{i\varphi}|H_1\rangle), \quad |\psi_D\rangle = \alpha|V_2\rangle + \beta|H_2\rangle.$$

The quantum system in front of the BPS is in state

$$|\psi_P\rangle \otimes |\psi_D\rangle \;=\; \frac{1}{\sqrt{2}}(|V_1\rangle + e^{i\varphi}|H_1\rangle) \otimes (\alpha|V_2\rangle + \beta|H_2\rangle) \;=$$

$$= \frac{1}{\sqrt{2}}(\alpha|V_1V_2\rangle + \beta|V_1H_2\rangle + e^{i\varphi}\alpha|H_1V_2\rangle + \beta e^{i\varphi}|H_1H_2\rangle).$$

The PBS transforms the inputs states according to Eqs. (3.5) and (3.6), thus the H polarized light goes through the PBS and the V polarized light is reflected. Output modes of PBS are denoted 3 and 4, see Fig. 3.5. $|V_1\rangle \longrightarrow |V_3\rangle, |H_1\rangle \longrightarrow |H_4\rangle, |V_2\rangle \longrightarrow |V_4\rangle, |H_2\rangle \longrightarrow |H_3\rangle$. The quantum state of the system behind the PBS reads

$$\frac{1}{\sqrt{2}}(\alpha|V_3V_4\rangle + \beta|V_3H_3\rangle + e^{i\varphi}\alpha|H_4V_4\rangle + \beta e^{i\varphi}|H_3H_4\rangle).$$

If the events where there is one photon at each port of PBS are post-selected the conditional state can be written as

$$|\omega\rangle \;=\; \frac{1}{\sqrt{2}}(\alpha|V_3V_4\rangle + \beta e^{i\varphi}|H_3H_4\rangle). \tag{3.16}$$

When two photons go into single output port the gate operation fails. The auxiliary system (the program qubit) is measured in the basis $|\varphi_\pm\rangle$, where $|\varphi_+\rangle = \frac{1}{\sqrt{2}}(|V\rangle + |H\rangle)$ and $|\varphi_-\rangle = \frac{1}{\sqrt{2}}(|V\rangle - |H\rangle)$, at output 3. The resulting quantum state of the data qubit is

$$|\vartheta_\pm\rangle \;=\; \langle\varphi_\pm|\omega\rangle = \frac{1}{2}(\alpha|V_4\rangle \pm \beta e^{i\varphi}|H_4\rangle).$$

If the photon is found in the basis state $|\varphi_+\rangle$ the data qubit state is changed to $|\vartheta_+\rangle$, thus the gate performs the required operation. But if the photon is found in the basis state $|\varphi_-\rangle$ the data qubit state is changed to $|\vartheta_-\rangle$, thus the gate performs the unwanted operation – these results are thrown out. Thus, this implementation of programmable phase gate yields 25% success probability.

3.6.2 Programmable phase gate with increased succes probability

We implement the optimal active version of the programmable phase gate. We use the electronic feed-forward to increase the success probability of the gate from 25% [2] to its theoretical limit of 50% [1]. Our quantum programmable phase gate is implemented using fibre optics components. The core of the gate is based on two interconnected fibre Mach-Zenhder interferometers

operating at a single photon level. Information is encoded into spatial modes of light. The basis states are $|0\rangle$ and $|1\rangle$ which represent the passage of the photon through the first and the second arm, respectively, see Fig. (3.6).

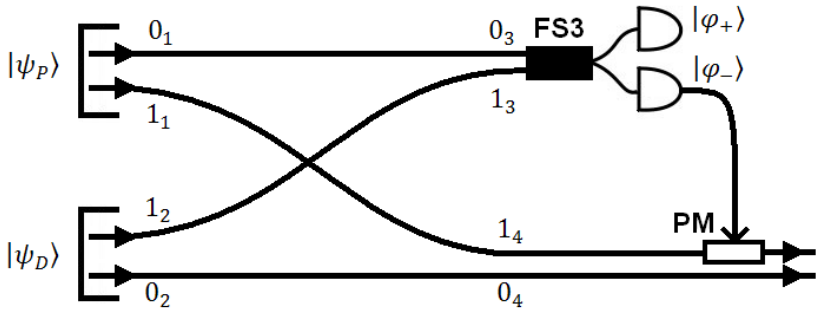

Figure 3.6: Scheme of the programmable phase gate using fibre optical components.

The idler photon enters the input fibre splitter (FS1) and the signal photon enters the input variable ratio splitter (VRS2), see Fig. 4.1. The program qubit $|\psi_P\rangle$ and data qubit $|\psi_D\rangle$ are encoded into the idler and signal photons using FS1 and VRS2 and phase modulator (PM),

$$|\psi_P\rangle = \frac{1}{\sqrt{2}}(|0_1\rangle + e^{i\varphi}|1_1\rangle), \quad |\psi_D\rangle = \alpha|0_2\rangle + \beta|1_2\rangle.$$

Thus, the initial state of the system is

$$|\psi_P\rangle \otimes |\psi_D\rangle \;=\; \frac{1}{\sqrt{2}}(|0_1\rangle + e^{i\varphi}|1_1\rangle) \otimes (\alpha|0_2\rangle + \beta|1_2\rangle) \;=$$

$$= \frac{1}{\sqrt{2}}(\alpha|0_1 0_2\rangle + \beta|0_1 1_2\rangle + e^{i\varphi}\alpha|1_1 0_2\rangle + \beta e^{i\varphi}|1_1 1_2\rangle).$$

After passing through the gate – through the swapping arms, see Fig. (3.6), the indices are changed according the output modes 3 and 4: $|0_1\rangle \longrightarrow |0_3\rangle, |1_1\rangle \longrightarrow |1_4\rangle, |0_2\rangle \longrightarrow |0_4\rangle, |1_2\rangle \longrightarrow |1_3\rangle$. The state of the entire system in front of the detecting part is

$$\frac{1}{\sqrt{2}}(\alpha|0_3 0_4\rangle + \beta|0_3 1_3\rangle + e^{i\varphi}\alpha|1_4 0_4\rangle + \beta e^{i\varphi}|1_3 1_4\rangle).$$

If we post-select the events there is one photon at each port 3 and 4 (FS3 and VRS4), the

resulting conditional state $|\omega\rangle$ can be written as

$$|\omega\rangle \;=\; \frac{1}{\sqrt{2}}(\alpha|0_3 0_4\rangle + \beta e^{i\varphi}|1_3 1_4\rangle). \tag{3.17}$$

Than we measure the auxiliary system (the program qubit) in the basis $|\varphi_\pm\rangle$, where $|\varphi_+\rangle = \frac{1}{\sqrt{2}}(|0\rangle + |1\rangle), |\varphi_-\rangle = \frac{1}{\sqrt{2}}(|0\rangle - |1\rangle)$ at the output 3

$$|\vartheta_\pm\rangle \;=\; \langle\varphi_\pm|\omega\rangle = \frac{1}{2}(\alpha|0_4\rangle \pm \beta e^{i\varphi}|1_4\rangle)$$

Due to the measurement on the program qubit the output state of the signal photon is modified.

If the photon is found in the basis state $|\varphi_+\rangle$ the data qubit state is changed to $|\vartheta_+\rangle$ and the gate performs the require operation. If the photon is found in the basis state $|\varphi_-\rangle$ the data qubit state is changed to $|\vartheta_-\rangle$ and the gate performs the incorrect operation. However we do not throw out these states but we convert them to the required states. We achieve this correction through the electronic feed-forward.

The feed-forward enables us to affect the output state of the data qubit according to the result of measurement on the program qubit. Thus the incorrect state is changed to required one by the added phase shift π to basis state $|1_4\rangle$.

$$|\vartheta_-\rangle = \frac{1}{2}(\alpha|0_4\rangle - \beta e^{i\varphi}|1_4\rangle) \quad \Longrightarrow \quad \frac{1}{2}(\alpha|0_4\rangle - \beta e^{i\varphi}e^{i\pi}|1_4\rangle) = \frac{1}{2}(\alpha|0_4\rangle + \beta e^{i\varphi}|1_4\rangle) = |\vartheta_+\rangle$$

Thus this implementation of the programmable phase gate has 50% success probability; it is equal to its theoretical limit.

4 Design of the experimental setup

We proposed the experimental setup of a linear-optical programmable single-qubit phase gate using two interconnected fibre optical MZ interferometers. We chose fibre optical implementation because of the feasibility of the feed-forward technique. We tested the electronic feed-forward last year in a fibre optical setup [12]. Encoding of the qubits into spatial modes of light was chosen because it is easier to implement in a fibre optical setup than polarization encoding as it is difficult to control polarization in optical fibres.

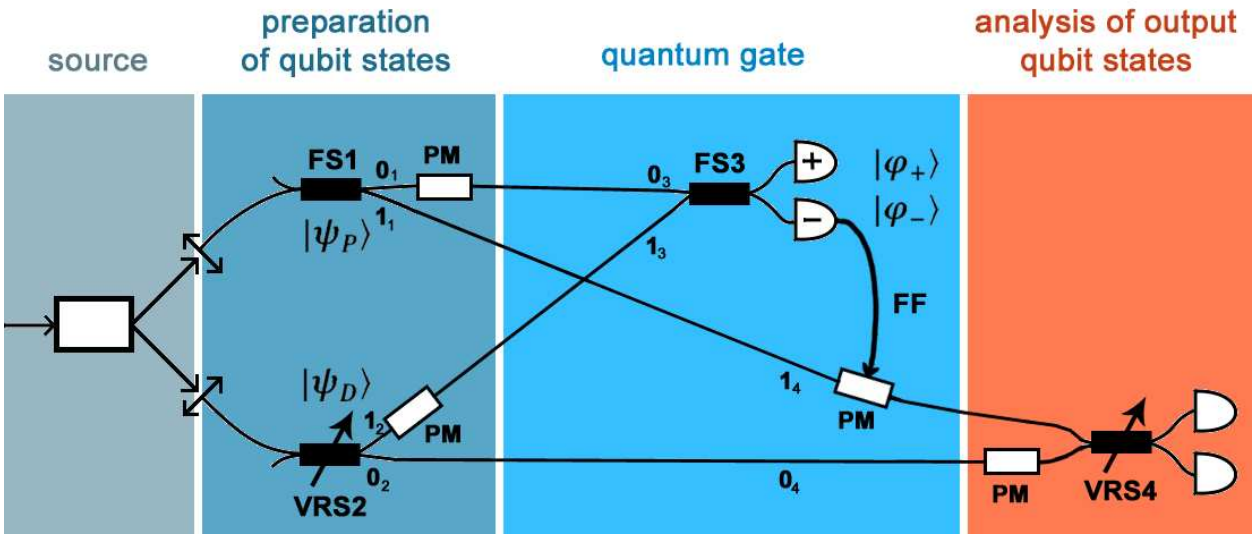

Figure 4.1: Scheme of the experiment, VRS – variable ratio splitter, FS – fibre splitter, PM –phase modulator, FF – feed-forward

Our experimental setup can be divided into several parts, see Fig. 4.1. The first is the source of time-correlated photons pairs (signal and idler photons) and coherent laser source of a probe beam. The second part is the qubit states preparation, where the quantum states of the data and program qubits are encoded into the signal and idler photons respectively. The third part consists of the quantum gate which uses the electronic feed-forward for correcting the improper states. And the last fourth part is the output analysis of the data qubit state.

For the sake of description, it is better to divide the setup into two interferometers – a short and a long ones. The short interferometer includes measurement on the auxiliary system (on the program qubit). The quantum state of the data qubit is modulated by the electronic feed-forward in the long interferometer. For better orientation we denote the particular arms and parts of the interferometers: arms 1 and 2, which are shared by both interferometers, Blue and Orange arms of the short interferometer and Yellow and Green arms of the long interferometer, see Fig. 4.2.

4.1 Influences of the losses on the gate operation

As we stated before, fibre optical components have relatively larger losses compared to bulk optical components. Here we analyze the influence of the losses on the operation of gate, see Fig. 4.2.

The program qubit $|\psi_P\rangle$ is encoded into the idler photon which passes through the arm 1 with

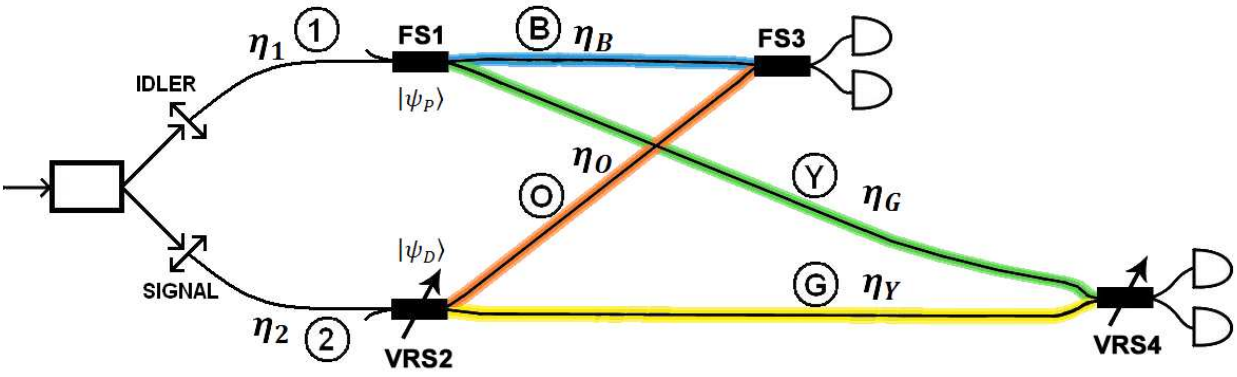

Figure 4.2: Simple scheme of the experiment, 1 – arm 1, 2 – arm 2, B – Blue arm , O – Orange arm, Y – Yellow arm, G – Green arm, η – efficiency (transmittance the part of interferometer arm),VRS – variable ratio splitter, FS – fibre splitter

efficiency η_1 and the data qubit $|\psi_D\rangle$ is encoded into the signal photon which passes through the arm 2 with efficiency η_2,

$$|\psi_P\rangle = \frac{1}{\sqrt{2}} \cdot \sqrt{\eta_1} \cdot (|0_1\rangle + e^{i\varphi}|1_1\rangle), \quad |\psi_D\rangle = \sqrt{\eta_2} \cdot (\alpha|0_2\rangle + \beta|1_2\rangle).$$

Here we adopt the notation where quantum states are not normalized to unity. Then measurements give the probabilities lowered due to losses, in fact the relative detection rates only. After encoding of the program and data qubits the initial state of the quantum system is

$$|\psi_P\rangle \otimes |\psi_D\rangle = \frac{1}{\sqrt{2}} \cdot \sqrt{\eta_1} \cdot (|0_1\rangle + e^{i\varphi}|1_1\rangle) \otimes \sqrt{\eta_2} \cdot (\alpha|0_2\rangle + \beta|1_2\rangle) =$$

$$= \frac{1}{\sqrt{2}} \cdot \sqrt{\eta_1\eta_2} \cdot (\alpha|0_1 0_2\rangle + \beta|0_1 1_2\rangle + e^{i\varphi}\alpha|1_1 0_2\rangle + \beta e^{i\varphi}|1_1 1_2\rangle).$$

The transformation of the gate is described by

$$|0_1\rangle \longrightarrow \sqrt{\eta_B}|0_3\rangle, \quad |1_1\rangle \longrightarrow \sqrt{\eta_G}|1_4\rangle, \quad |0_2\rangle \longrightarrow \sqrt{\eta_Y}|0_4\rangle, \quad |1_2\rangle \longrightarrow \sqrt{\eta_O}|1_3\rangle,$$

where η_B, η_G, η_Y and η_O are efficiency of the Blue, Green, Yellow and Orange arms, respectively. The state of the entire system before entering the detector is

$$\frac{1}{\sqrt{2}}\sqrt{\eta_1\eta_2}(\alpha\sqrt{\eta_B\eta_Y}|0_3 0_4\rangle + \beta\sqrt{\eta_B\eta_O}|0_3 1_3\rangle + e^{i\varphi}\alpha\sqrt{\eta_G\eta_Y}|1_4 0_4\rangle + \beta e^{i\varphi}\sqrt{\eta_G\eta_O}|1_3 1_4\rangle).$$

We post-select the events when each of the output ports 3 and 4 is populated by single photon only. The resulting conditional state reads

$$|\omega\rangle \;=\; \frac{1}{\sqrt{2}}\sqrt{\eta_1\eta_2}(\alpha\sqrt{\eta_B\eta_Y}|0_30_4\rangle + \beta e^{i\varphi}\sqrt{\eta_G\eta_O}|1_31_4\rangle). \tag{4.1}$$

Then we measure the auxiliary system (the program qubit) at the output 3 in the basis $|\varphi_\pm\rangle_3$, where $|\varphi_+\rangle_3 = \frac{\eta_D}{\sqrt{2}}(|0\rangle + |1\rangle)$ and $|\varphi_-\rangle_3 = \frac{\eta_D}{\sqrt{2}}(|0\rangle - |1\rangle)$, where η_D means detection efficiency. The output state of the data qubit is

$$\langle\varphi_\pm|\omega\rangle \;\;=\;\; \frac{\eta_D}{2}\sqrt{\eta_1\eta_2}(\alpha\sqrt{\eta_B\eta_Y}|0_4\rangle \pm \beta e^{i\varphi}\sqrt{\eta_G\eta_O}|1_4\rangle) \;\neq\; |\vartheta_\pm\rangle \tag{4.2}$$

We can see that the efficiencies η_1, η_2 of the arms 1 and 2, which are shared by both interferometers, change only the norm of the state but do not change the state itself. The efficiencies η_B, η_O, η_G and η_Y change the quantum state of the output data qubit.

If the relation

$$\eta_B \cdot \eta_Y = \eta_O \cdot \eta_G = \Gamma^2. \tag{4.3}$$

is fulfilled the output quantum state of the data qubit is proportional to the ideal state

$$|\vartheta_\pm\rangle \approx \sqrt{\eta_1\eta_2}\Gamma\,|\vartheta_\pm\rangle$$

.

We now discuss the losses with regard to the short and long interferometers, see Fig. 4.2. We suppose that coherent light is divided 50:50 (on input PBS of both interferometers – the light source will be discussed later). Then we also suppose that the splitting ratios of outputs beam splitters FS3 and VRS4 are 50:50. And as we know from the description of the MZ interferometer – if input and output beam-splitters are both 50:50, then the visibility is affected only by the losses in interferometer arms. If we want unit visibilities at both output ports the losses in both arms must be equal,

$$\begin{aligned} \text{the short interferometer:} \quad & \eta_1 \cdot \eta_B = \eta_2 \cdot \eta_O, \\ \text{the long interferometer:} \quad & \eta_1 \cdot \eta_G = \eta_2 \cdot \eta_Y. \end{aligned}$$

The condition which is implied by these two equations is $\frac{\eta_Y}{\eta_G} = \frac{\eta_O}{\eta_B}$. As we can see, it is the same condition as the one in Eq.(4.3). Thus if we want to adjust the programmable phase gate

to do its operation correctly we have to align both interferometers in the setup to their maximum visibilities – balancing losses in the interferometers arms.

4.2 Influences of the phase shift on the gate operation

Here we extend our previous analysis of the gate to the influence of phase shifts in interferometers' arms. We suppose that each arm induces the efficiency as well as an extra phase shift.

The short interferometer possesses the additional phase shifts $e^{i\theta_B}$ and $e^{i\theta_O}$, the indices B and O correspond to arms Blue and Orange. The long interferometer has the additional phase shifts $e^{i\theta_G}$ and $e^{i\theta_Y}$, the indices G and Y correspond to arms Green and Yellow. Thus after the measurement on the auxiliary system (the program qubit) in the basis $|\varphi_\pm\rangle$, where $|\varphi_+\rangle = \frac{1}{\sqrt{2}}(|0\rangle + |1\rangle)$ and $|\varphi_-\rangle = \frac{1}{\sqrt{2}}(|0\rangle - |1\rangle)$ at output 3 the output state of the data qubit is

$$\langle\varphi_\pm|\omega\rangle \;=\; \frac{1}{2}\cdot\sqrt{\eta_1\eta_2}\cdot(\alpha\cdot\sqrt{\eta_B\eta_Y}\,e^{i\theta_B}\,e^{i\theta_Y}\cdot|0_4\rangle \pm \beta e^{i\varphi}\cdot\sqrt{\eta_G\eta_O}\,e^{i\theta_G}\,e^{i\theta_O}\cdot|1_4\rangle) \neq |\vartheta_\pm\rangle$$

We suppose that the losses in the interferometers' arms are compensated according to the condition in Eq. (4.3). Then the state data qubit is:

$$\frac{1}{2}\cdot\sqrt{\eta_1\eta_2}\Gamma\,e^{-i(\theta_B+\theta_Y)}\cdot(\alpha\cdot|0_4\rangle \;\pm\; \beta e^{i\varphi}\,e^{i(\theta_{short}+\theta_{long})}\cdot|1_4\rangle),$$

where θ_{short} and θ_{long} are phase shifts in the arms of the short and the long interferometer, respectively, $\theta_{short} = \theta_O - \theta_B$ and $\theta_{long} = \theta_G - \theta_Y$. If the phase shifts in the arms of the interferometers are equal to zero, $\theta_{short} = 0$ and $\theta_{long} = 0$, we obtain the data qubit in the required state

$$\frac{1}{2}\cdot\sqrt{\eta_1\eta_2}\Gamma\,e^{-i(\theta_B+\theta_Y)}\cdot(\alpha\cdot|0_4\rangle \;\pm\; \beta e^{i\varphi}\cdot|1_4\rangle) \;=\; \sqrt{\eta_1\eta_2}\Gamma\,e^{-i(\theta_B+\theta_Y)}\cdot|\vartheta_\pm\rangle.$$

To ensure a successful operation of the gate, stable phase has to be maintained in both interferometers. Active correction of phase has to be performed before each gate operation. It is provided by an automatic stabilization procedure that checks and corrects the phase (it will be described later).

Various mechanical effects such as air circulation or acoustic vibrations and temperature

fluctuations cause a phase drift in the interferometers' arms. Therefore, it is also necessary to mechanically isolate the setup for better passive stability.

5 Components

5.1 Light source

In our source there are conveniently integrated both the source of time-correlated photons and probe laser diode, see Fig. (5.1). We have a possibility to switch between them using choppers (VR, VB).

5.1.1 The parametric down conversion source of time-correlated photons

The source of correlated photons produces photon pairs with a central wavelength of 814 nm. It utilizes type-2 parametric down-conversion (PDC) in a 2 mm BBO crystal which is tilted for degenerate collinear generation. Pumping is provided by a 50 mW laser diode (BLD) at 407 nm. Group velocity dispersion and transversal walk-off are compensated by another BBO crystal, which is 1 mm thick. Depending on the requirements of our experiment we are able to increase visibility of Hong-Ou-Mandel dip by placing an interference filter (IF) in the setup. This, however, decreases our coincidence rate, as summarized in the table below, see Tab. 1 [14]. The PDC source was built by I.Straka and M. Ježek. The generated horizontally polarized signal photons

Table 1: Table of characteristics of the source of time-correlated photons; FWHM IF – full width in half maximum of interference filter, CR – coincidence rate , VIS – visibility of Hong-Ou-Mandel dip

FWHM IF [nm]	CR $[s^{-1}]$	VIS [%]
without IF	45000	86
10	19000	97
2	2500	99

and vertically polarized idler photons are separated by PBS (input PBS of the short and the long interferometers). Then the photons are coupled into fibres. We have also a possibility to block light entering into the idler or signal input coupling lenses (IICL, SICL) using flippers (FGB, FOY).

- Pumping laser diode – 50 mW at 407 nm, Cube 1069413 from Coherent S/N: 99867301

- IF – central wavelength 814 nm FWHM 2 nm – from Androver (814±1) nm
- BBO – beta-barium borate or β-BaB_2O_4, type 2, cut $\Theta = 42.7$deg, 2 mm thick

5.1.2 Probe laser diode

The probe laser diode is connected into the light source through the dichroic mirror which transmits red light (814 nm) and reflects blue light (407 nm), see Fig. 5.1. This part of the source we can use in two regimes. The first regime is strong signal, it means the full power of ca. 300 μW directly from laser diode is used. For detection PIN photo diodes or power meters are used. The second regime is weak coherent signal. In this regime the laser diode is attenuated and the light signal is detected by single photon detectors. We use this signal with count rates of approfimately million photons per second mainly for adjustment and active stabilization of our experiment.

- The laser diode – central wavelength 814 nm, FOB-01-3s-5/125-810-S-L from OZ OPTICS.

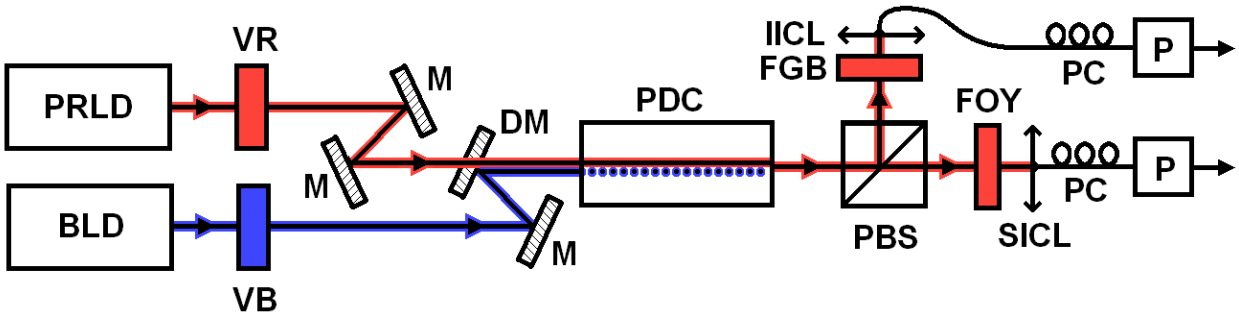

Figure 5.1: Scheme of the light source; PRLD – probe red laser diode, BLD – blue laser diode, VR, VB – choppers, DM – dichroic mirror, M – mirror, PDC – parametric down conversion, PBS – polarizing beam splitter, IICL, SICL – idler, signal input coupling lenses, FGB, FOY – flippers, PC – polarizing controller, P –polarizer

5.2 Choppers and Flippers

Choppers and flippers are devices which enable us to block the passing light beam in controlled way.

(a) Chopper (b) Flipper

Figure 5.2: Photos of chopper and flipper

5.2.1 Flipper

The motorized filter flipper from Thorlabs is used without filter but with black aluminium foil instead, thus it is used as beam stop. The flip operation is controlled by an external signal. The trigger is a TTL logic with pulse high 5 V. The flipper toggles between two perpendicular positions with each TTL pulse, see Fig 5.2b. The flip time is shorter then 0.5 s.

In our setup we use two flippers. They are placed in front of signal and idler input coupling lenses. They are used when a splitting ratio of variable ratio splitters is automatically set or when we balance losses in interferometers' arms.

5.2.2 Chopper

The step motor with slotted chopper wheel is used, see Fig 5.2a, which is external triggered by TTL puls 5 V high. Its switching time is shorter, but its operating temerature is really high and the temperature fluctuations induce phase drifts in our interferometer as was mentioned. Because of it, we placed the choppers out of our interferometers. They toggle between probe laser diode and photon pairs.

We measured the toggle time of the chopper and the flipper and we found that the chopper is

faster inspite of damped oscillation, see Fig 5.3a. The flipper has no oscillations and can be much faster in one direction of its flip action, see Fig 5.3b. As will be mentioned, for our aplications the flippers are more convenient than choppers.

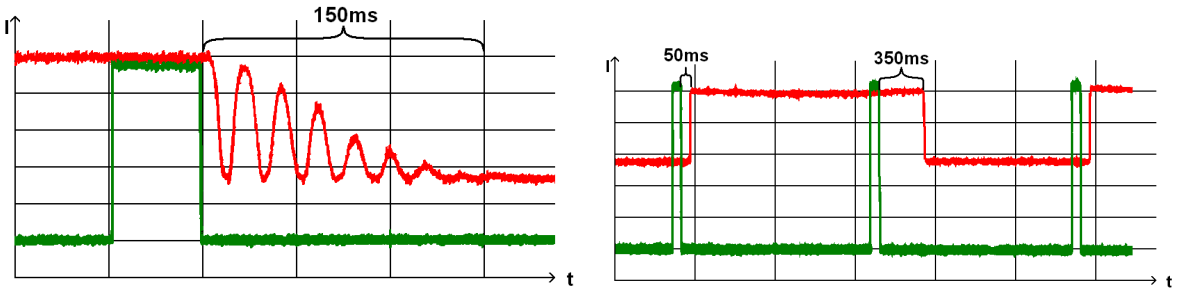

(a) Chopper's toggle time (50 ms/div) of approximately 150 ms

(b) Flipper's flip time (500 ms/div) of approximately from 50 to 350 ms

Figure 5.3: Comparison of Chopper's and Flipper's toggle time, red line – intensity of detect light, green line – trigger puls [50ms]

All choppers and flippers are controlled electronically by MATLAB environment through multiple channel Advantech digital output/input card (PCI-1723). Through the digital outputs we send TTL pulses of 5 V and in this way we switch between light sources or we block signal coming to input signal and idler coupling lenses. We have also implemented programs such as "choppers passability test" and "flippers passability test", which set choppers or flipper to position when light beams pass through. These programs are based on measurement of count rates.

- motorized flipper mount MFF001, from Thorabs [24]

5.3 Optical fibre

We use single-mode optical fibre for wavelength 814 nm, HP 780, from fused silica. The refractive index of fused silica for this wavelength is approximately 1.453.

- Single-Mode Fibre MFD5μ HP780, from Nufern [29]

5.4 Polarization controller (PC)

Polarization controller is utilized for changing polarization states of light in optical fibres in controlled way. The polarization of light in optical fibre is changed when the fibre moves or bends etc. thus the mechanical stress induces birefringence in the fibre. The light waves in such medium

are split into two orthogonally polarized waves and each of them feels different refractive index, which causes distortion of polarization state during the propagation in fibre.

In this way, we can create phase retardation between the orthogonally polarized waves which corresponds to quarter or half wave plates. The specific radius of fibre loop creates the require phase shift. One loop approximatelly corresponds to quarter-wave plates and two to half-wave plates. Thus PC consists of fibre loops in spatial movable holder where the fibre is fastened typically in order 1, 2, 1 turns ($\lambda/4$, $\lambda/2$, $\lambda/4$). Any polarization state can be reproduced, when the fibre loops are rotated along the holder axis. The PC is also called "bat ears", see Fig.(5.4).

Figure 5.4: Photo of pollarization controller

- polarization controller FPC030, from Thorlabs

5.5 Polarizer (P)

Linear polarizer is a passive optical device which changes the general polarization state of light to linear polarization state of light. It transmits all components of electric field, which are parallel with the linear polarization and it blocks all perpendicular components. We use two types of polarizers in out setup, bulk cube and integrated fibre polarizer.

The integrated fibre polarizers are used at the output of light source, see Fig. 5.1, thus in front of the state preparation. It is very convenient for adjustment of entire setup to have a stable incoming polarization inside the interferometers' arms, because of the polarization dependent losses in them. In front of the polarizers, there are polarization controllers to optimize their transmittances. The using of bulk polarizers cube will be discussed later. The combination of PC and P can be also used as attenuator, see Fig. 5.5.

- Fibre polarizer – FOP-01-33-810-S-S, S/N: 97359-1, OZ OPTICS, transmission 79,8%
- Fibre polarizer – FOP-01-33-810-S-S, S/N: 97359-2, OZ OPTICS, transmission 74,3%

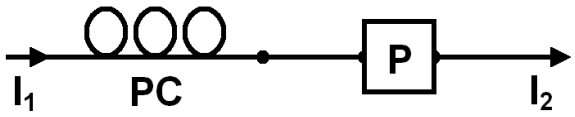

Figure 5.5: Setup of polarization controller (PC) and polarizer (P) , I_1, I_2 – input, output intensities of light respectively, $I_1 > I_2$

5.6 Phase Modulator (PM)

Electro-optical phase modulator is a device which enables us to implement fast phase shift in the interferometer's arm. The PM is based on linear Pockels effect. When the intensity of electric field, which is applied on the nonlinear crystal of lithium niobate, is increased then the refractive index of the crystal grows. The optical path of PM is longer. Many procedures as active stabilization, measurement of visibility and the feed-forward implementation exploit PM.

In our experiment we use four phase modulators from EOSPACE. All modulators are pigtailed by polarization maintaining fibres. It is necessary to keep the right polarization because of the phase modulator birefringence. It means the half-wave voltage is different for different polarization components of light which propagates inside of PM. One type of phase modulator contains an integrated polarizer (PM+P), see Fig. 5.6, and another type not (PM), see Fig. 5.7. The setup was designed in a way, that phase modulator and polarizer are placed in each arm, see Figs. 6.1 and 6.2.

- arm **B:** PM+P – PM-OK5-00-PFU-PFUP-830-S, S/N:73931 – stabilization of short interf.
- arm **O:** PM – PM-OK1-00-PFU-PFU-830-S, S/N:75815
- arm **Y:** PM+P – PM-OK5-00-PFU-PFUP-830-S, S/N:73932 – stabilization of long interf.
- arm **G:** PM – PM-OK1-00-PFU-PFU-830-S, S/N:75835 – feed-forward

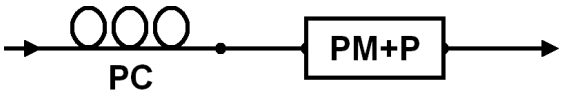

Figure 5.6: Scheme of connection – polarization controller (PC) with phase modulator with integrated polarizer (PM+P)

Table 2: Table of characteristics of phase modulators

phase modulators	input fibre length [mm]	body [mm]	output fibre length [mm]	insertion loss [dB]	half-wave voltage [V]
PM+P S/N:73931	1253	90	1260	4.1	1.444
PM S/N:75815	1235	90	1241	2.3	1.5475
PM+P S/N:73932	1258	90	1257	4.5	1.440
PM S/N:75835	1090	90	1090	1.7	1.455

We controlled the phase modulators by computer through multiple channel Advantech analog output card (PCI-1723 HG). We need to know the precise values of half-wave voltages of phase modulators to our programs implemented a correct phase shifts. The method of determining half-wave voltage is described in [19] and [12].

5.7 Air gaps

In our setup there are implemented two types of air gaps, all of them have adjustable length. Since it is almost impossible to build interferometer with equally long arms, the compensation of path difference is ensured by the adjustable gap. Our interferometers have several meters long arms and because of it, we placed the adjustable gap inside each arm, such that each interferometer contains both types of air gaps. The transmission of each gap is ca. 85%.

5.7.1 Shorter air gap with motorized stage

This type of air gap consists of output coupling lens, two mirrors for alignment and input coupling lens. The output coupling lens is mounted on a computer-controllable motorized stage. We use it for automatic scanning of the air gap, thus finding maximum visibility of the probe signal or Hong-Ou-Mandel dip of the photon pairs. See the air gaps in Blue and Yellow arms in Fig. 6.2.

5.7.2 Longer air gap with corner reflector and manual stage

This type of air gap consists of output coupling lens, two half-wave plates, quarter-wave plate, polarizer, four mirrors and input coupling lens. Two mirrors are mounted on a manual mechanical stage perpendicular to each other, thus the shift of the stage induces two times longer change of

optical path. It is used for approximate alignment of maximum visibility with the strong probe signal.

The quarter-wave plate and half-wave plates, behind the polarizer are used for adjusting polarization overlap in the output fibre-splitter of MZ interferometer. The adjustment of polarization overlap is more comfortable with this sequence of bulk wave plates than with fibre polarization controller, because it is more repeatable and not so heuristics. See the air gaps in schemes of Green and Orange arms Fig. 6.2.

The last important part of long air gap is the sequence of output coupling lens, half-wave plate and polarizer, see Fig 5.7, which substitutes the integrated polarizer of PM, see Fig 5.6. The correct angle of rotation of half-wave plate sets the right polarization state of light so that only the light components which were properly modulated by PM pass through the polarizer. If the angle of rotation of half-wave plate is incorrect and voltage is applied on PM, we observe modulated fringes. After the setting of half-wave plate and reaching harmonics interference pattern we optimize the polarization by fibre polarization controller before PM for maximum transmittance.

- Mirrors – Broadband Dielectric Mirrors from Thorlabs, BB1-E03, BB1-E02 [25]
- Lenses – Molded Glass Aspheric Lenses from Thorlabs, C220TME-B [27]
- Half plates and quarter wave plates – anti-reflection coated, designed for 800 nm and 810 nm, from EKSMA
- Bulk polarizers – anti-reflection coated dielectric PBS, from EKSMA and CVI

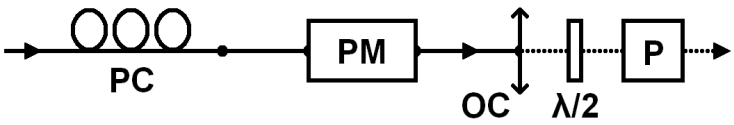

Figure 5.7: Scheme of substitution of integrated polarizer (P) of phase molulator (PM), PC – polarization controller, $\lambda/2$ – half-wave plate, OC – outpul coupling lens

5.8 Detectors

In our experiment we use two types of detectors. PIN photo diodes for detection of strong signal from the probe laser diode and single-photon detectors for detection of photon pairs from PDC and weak coherent state from attenuated probe laser diode.

5.8.1 PIN photo diodes

The measured data from PIN diode can be processed by oscilloscope or by computer through multiple channel Advantech analog input card (PCI-1710 HG). Due to better time resolution, functionality and graphical interface we mainly use the oscilloscope LeCroy WavePro 715Zi.

5.8.2 Single-photon detectors

We use single-photon detectors – silicon APDs (Avalanche Photo diodes) operated in Geiger mode, the output signal of the detector consists of positive logic TTL pulses of 4.5V. The single-photon detectors have several important parameters which we have to take into account.

A dead time of detector is the minimum possible time between two distinguishable detections. Our detectors have the dead time ca. of tens of nanoseconds [18]. Efficiency of our detectors is around 50% for 814 nm [23]. If we want to compare data obtained from the detectors, we need to know relative efficiencies of the detectors, see Tab.3. Other important parameter of the detectors is dark count rate - the noise of detectors. Further, a duration of the detector response has to be known if we want to set a proper timing of feed-forward or set the coincidence logic, see Tab.3, [21, 12].

- PIN diodes – silicon photo diodes, DET36A and PDA36A, from Thorlabs [?]
- Digital osciloscope – 4 channel 1.5 GHz, 10Gb/s, Wave Pro 715Zi, from LeCroy [28]
- Array of single-photon detectors – SPCM-AQ4C from Perkin Elmer Optoelectronics
- Single-photon detector – SPCM AQR-14FC 13610 from Perkin Elmer Optoelectronics

Table 3: Table of the single-photons detectors' parameters

		relative efficiency	dark counts $[s^{-1}]$	duration of detector response [ns]
SPCM-AQ4C	CH0	0.9848	440	35
	CH1	0.7326	195	40
	CH2	1	386	33
	CH3	0.9823	394	33
SPCM AQR-14FC	CH	0.8224	358	17

5.9 Counters and coincidences logic

5.9.1 Counters

- QUAD – Ortec 974 100 MHz Quad Counter/Timer
- QUAD2 – Ortec 974 100 MHz Quad Counter/Timer
- DUAL – Ortec Dual Counter/Timer

Both QUAD and QUAD2 have four input channels, the first CH0 is usually employed as a timer to preset counting time. But we need to use 9 counter channels and thus we use also DUAL counter with other two channels and we set QUAD and QUAD2 to external timer from DUAL counter. The pulses from the detectors are converted by an inverting transformer before they enter into counter from positive voltage TTL pulses to NIM negative pulses. The counters count the pulses per specified unit of time. The counters are controlled through a serial ports (RS-232) using the MATLAB environment.

Table 4: Table of detector's channels; chan. – channel, cr. – count rate, coinc. – coincidences

QUAD				QUAD2			DUAL	
CH0 chan.1	CH1 chan.2	CH2 chan.3	CH3 chan.4	CH1 chan.5	CH2 chan.6	CH3 chan.7	CHA chan.8	CHB chan.9
cr. output1 long int.	cr. output2 long int.	cr. output1 short int.	cr. output2 short int.	coinc.	coinc.	coinc.	coinc.	coinc.
L1	L2	S1	S2	S1-L1	S1-L2	S2-L1	S2-L2	S1-S2 or L1-L2

CH0	CH2	CH3	CH
single-photons detectors			

5.9.2 Coincidences logic

To measure coincidences we have to use a coincidence logic. First we set the same arrival time of all pulses. Second the width of the pulses is reduced from ca. 30 ns to ca. 2.5 ns by discriminator, then the pulses are replicated. And finally, we use coincidence logic and the outputs are counted by conters, see Fig. 8.2.

- dual delay 792 – Dual passive delay module 0.5÷63.5 ns per section, from Phillips Scientific

- discriminator 708 – Octal 300MHz discriminator, from Phillips Scientific
- fan out 748 – Octal bipolar linear fan-out, from Phillips Scientific
- quad Logic 754 – Quad 300MHz four-fold majority logic unit, from Phillips Scientific

5.10 Feed-forward

As was stated the efficiency of the probabilistic quantum gate is not unity. Several methods were suggested how to improve the success probability of linear optics gates, one of them is feed-forward technique [4]. Our feed-forward implementation uses a direct signal from a single photon detector and through a voltage divider the output data qubit state is modified via a fast electro optical modulator.

The electric feed-forward was tested last year at single-qubit MZ interferometer [12], see Fig. 5.8. It is built form the single-photon detector, a variable voltage divider, appropriately long coaxial cable (according the timing) and the phase modulator.

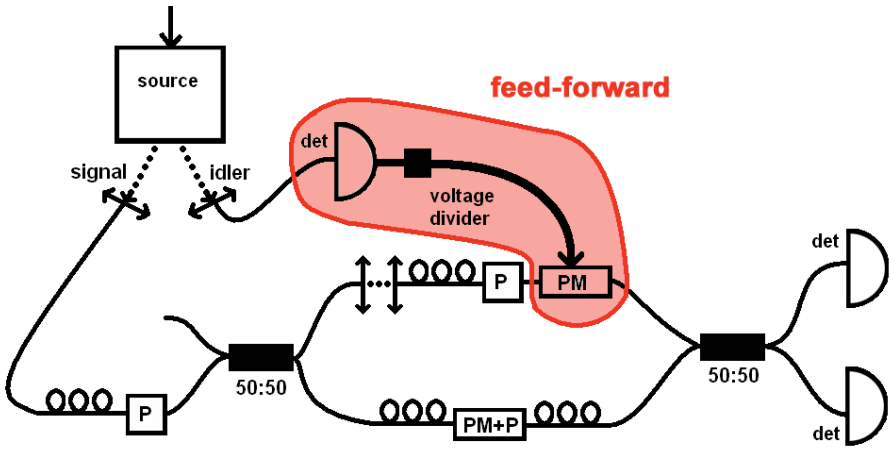

Figure 5.8: Scheme of the setup where the feed-forward was successfully tested

It is necessary to precisely set the variable voltage divider to modify the voltage level of the puls from single photon detector to half-wave voltage of the phase modulator. We use the single-photon detector SPCM AQR-14FC 13610 from Perkin Elmer Optoelectronics, because of its short response time 17 ns and the puls width is 30 ns. We want to modulate the data qubit in the middle of this puls (via fast electrooptical modulator).

Thus the time when the data qubit travels through the long interferometer to phase modulator in Green arm has to be equal to the time when the program qubit passes the short interferometer, is detected, the high of the puls is appropriately modified and then the puls is applied to the phase modulator.

So the time delay of feed-forward loop is compensated by delay lines implemented into the long interferometer's arms. For better orientation see Figs. 6.1 or 6.2.

5.11 Fibre splitter (FS) and variable ratio splitter (VRS)

We use fibre splitters 2 x 2 with two inputs and two outputs. The splitting ratio depens on the length of joint part of the two fibres (the part, where cores of fibres are in touch and where the transfer of energy occurs) and on the wavelength of the light.

We use two FS from Sifam Fibre Optics in our setup, we denote them as FS1 and FS3. From our equipment, we tried to choose FSs with splitting ratio close to 50:50 for wavelength 814 nm. The length of inputs and outputs fibres are indicated in Tab. (5).

- input fibre-splitter FS1 – SIFAM 01199313, splitting ratio 47.38%:52.62% for 814 nm
- output fibre-splitter FS3 – SIFAM 01176017, splitting ratio 53.27%:46.73% for 814 nm

We also use another two fibre splitters with variable splitting ratio (VRS) from Canadian Instrumentation and reasearch, Ltd., Model 905E. There are two possibilities, how to change the splitting ratio. The first possibility is rotation of micrometric screw. The second possibility is to use a piezo driver (Model 914-2 Piezo Controller with 905E, 916 Piezo out) [22], but the splitting ratio depends on the initial position of the micrometric screw. The input voltage of the piezo controller 916 Piezo Out is from 0V to +5V. It enables us to set the required splitting ratio of VRS. Manufacturer states that +3V is the maximum necessary voltage to change the splitting ratio from 100:0 to 0:100 or vice versa.

One of the problems with setting the splitting ratio is that both the methods have hysteresis behavior. We observed and characterized this behaviour at one output port of VRS. At the second port of VRS we observed the same bahaviour but maximum and mimunum were changed, see Fig. 5.9. Another problems with setting the splitting ratio of VRS is its dependence on the speed of voltage apllication.

- input variable ratio splitter VRS2 – S/N: 6516-1, Piezo Controller S/N:

- output variable ratio splitter VRS4 – S/N: 5860-1, Piezo Controller S/N:

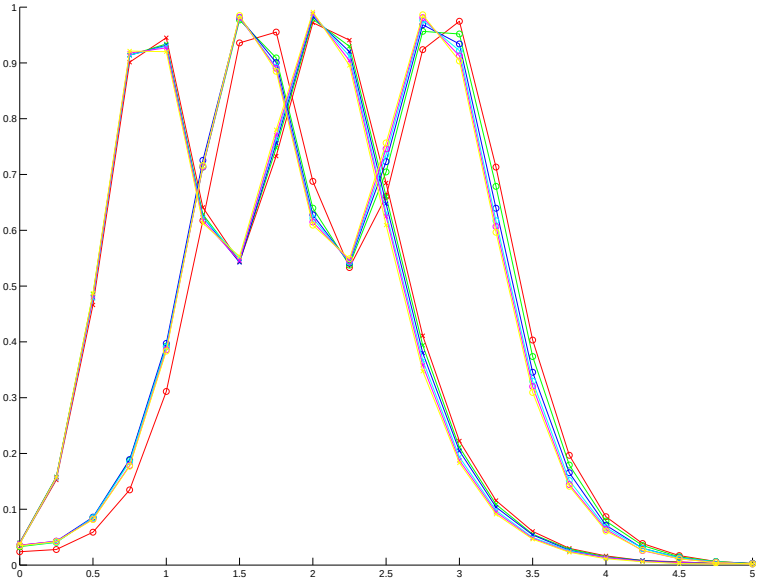

Figure 5.9: Graph of hysteresis behavior of VRS4; x-axis – voltage, y-axis – splitting ratio – reflectivity, circles – increassing voltage from 0V to +5V, crosses – decreassing voltage from +5V to 0V, different colours denote different speeds of setting the voltage, red is the fastest and yellow the slowest

Table 5: Parameters of Fibre splitter (FS) and Variable ratio splitter (VRS)

	length [mm]			
input/output	FS 01199313	FS 01176017	VRS 6516-1	VRS 5860-1
fibre A	1008	1009	823	1045
fibre B	1010	1007	1014	1045
fibre X	1003	1007	1010	1018
fibre Y	1005	1009	999	1018
body	80	80	70	70

We wrote several programs for controlling, setting and testing of the splitting ratio of VRS. The main reason why we need to control the splitting ratio and to know its time evolution is that we want to do tomographic measurement of the gate. We have to set all measurement basis

using variable ratio splitters and phase modulators. A lot of our programs were written for two types of detectors and thus for two type of data acquisition: strong and weak signal. We use strong light signal and PIN photodiodes as detector. The data are loaded through interface of PCI-1710 HG Advantech into computer (Max. input voltage $\pm$15V, resolution 12-bit, 1 step is 0,0073V). Because of better time resolution, functionality and graphical interface we mainly use the osciloscope LeCroy. Despite it, we have designed several programs, which use interface of Advantech card.

But the most programes was written for weak signal, thus for comunication with counters, because of the thomography. We wrote programs for automatical setting of the splitting ratios of input and output variable ratio splitter, VRS2 and VRS4. The core of this programs is different but the stucture around is very similar. First the VRS has to be mechanichaly set to splitting ratio 0:100 and then our procedure is applicable.

The program measures the calibration curves of VRSs and then they set the required splitting ratios. Also the speed and steps of the control voltage were optimized. The procedure has to be relatively slow if we want to have stable splitting ratio. (For more detail see programs on CD.)

6 Experimental setup

6.1 Layout of the experiment

The first was an idea obout fibre optical programmable phase gate with electronic feed-forward. Then we defined all components which are necessary for the operation of the gate and its full tomographic characterization and we specified their optimal interconnection in the setup. We measured characteristics and parameters of all the components. Than we started with timing of feed-forward. When lengths of air gaps were approximately estimated we ordered the fibre optical delay lines. Acording their actual lengths we finally designed the lengths of the air gaps, see Fig. 6.1. The air gap components and all fibre interconnections were aligned to maximum transmittance. Despite of it, the total efficiency of the setup is between 10%-13% (for more detail see the attached program " `kontrola_delek_ramen_p.m` ").

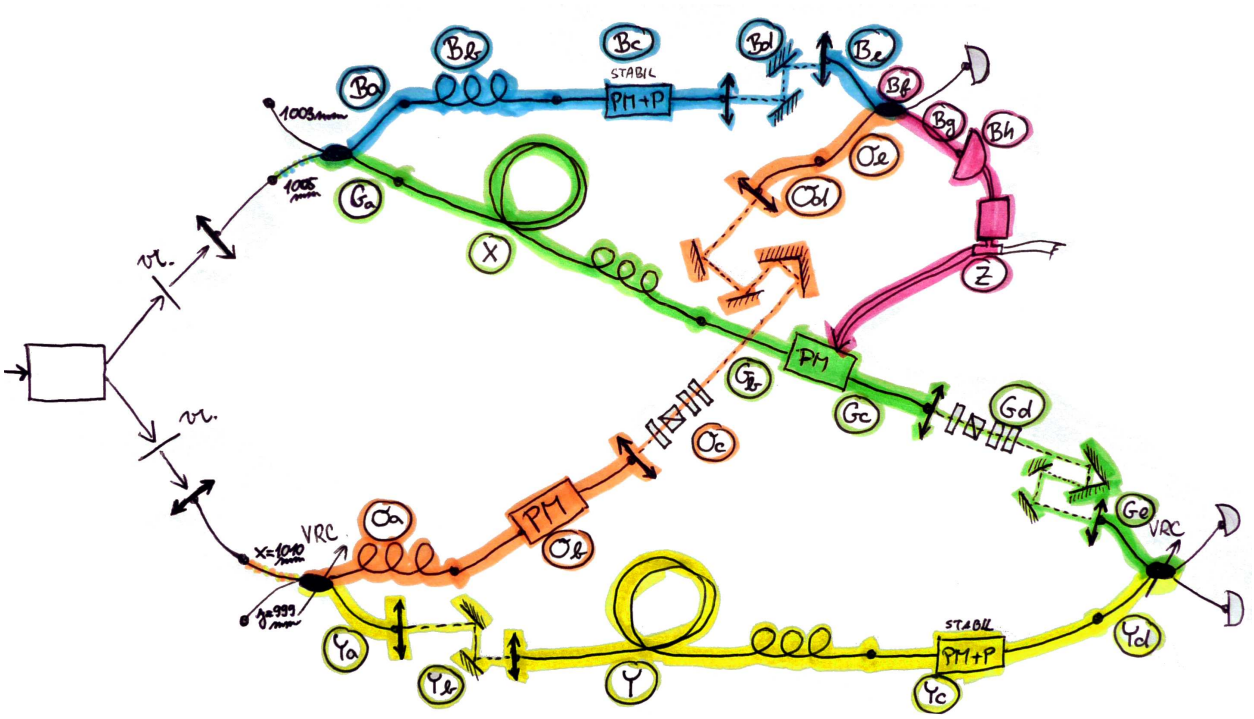

Figure 6.1: Sketch of the entire experiment

6.2 Arms of short and long interferometers

The significant parameters of the arms are their lengths. The Blue and Orange arms of short interferometer are 5665 mm long (optical fibre equivalent) and the Green and Yellow arms of long interferometer are 16678 mm long (optical fibre equivalent). The arms 1 and 2 which are shared by both interferometers are approximately 4900 mm long. The actual lengths slightly depends on PDC source setting.

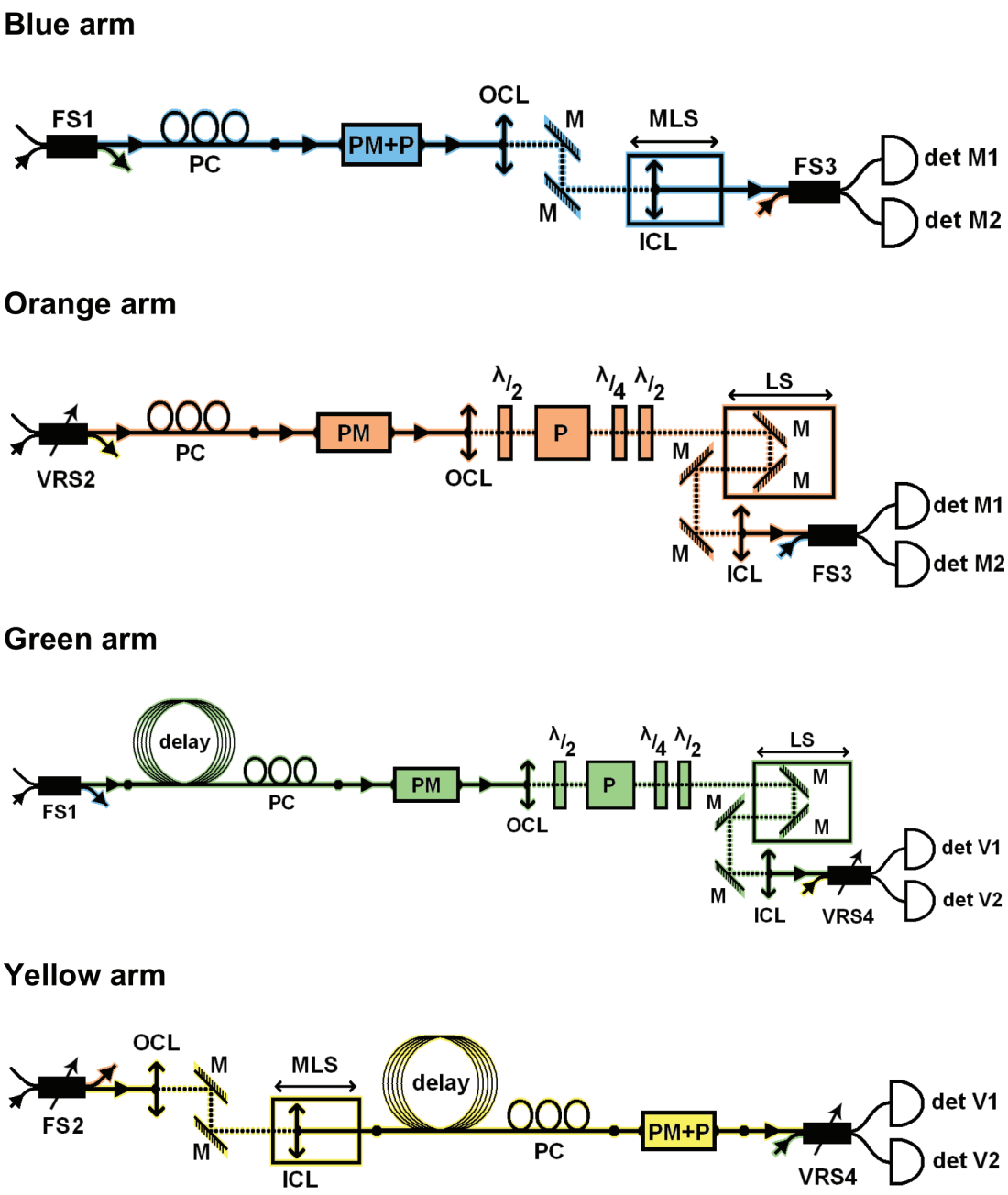

Figure 6.2: Scheme of the Blue, Orange, Green and Yellow arms; PC – polarization controller, M – mirror, P – polarizer, PM – phase modulator, PM+P – phase modulator with integrated polarizer, OCL and ICL – output and input coupling lenses, det – detector, FS – fibre splitter, VRS – variable ratio splitter, delay – delay line, LS – manual linear stage, MLS – rotorized linear stage, $\lambda/2$ and $\lambda/4$ – half and quarter wave plates

7 Stabilization

7.1 Passive stabilization of interferometers

The passive stabilization of both interferometers is provided by a polystyrene box which partially isolates the setup from the air circulation, acoustic vibrations and temperature fluctuations. Moreover, the whole experiment is built on an optical table which lies on pneumatic supports which attenuate various mechanical effects. Because the refractive index of fibers is very sensitive to temperature fluctuations, we have employed an extra isolation around the fibre optical delay lines in the long interferometer. The fibres are coiled onto an aluminum cylinder and covered with an isolating foil.

But this does not solve the problem completely. A better passive stability will enable the gate to do the required operation for a longer time, if we also employ an active correction of phase which has to be performed before each gate operation.

7.2 Active stabilization of interferometers

To ensure a successful operation of the logical gate, stable phase has to be maintained in both fiber MZ interferometers. We use an automatic stabilization procedure that checks and corrects the phase by means of electro-optical modulators. The principle of the stabilization procedure is the same here as in the previous part of the experiment, where feed-forward was demonstrated [12] ([20]).

For each interferometer, fringes are measured for both outputs. Visibility, minima and maxima values are read from the results. The electro-optical modulator voltage value U_{min} corresponding to a minimum on one of the outputs of the interferometer, because stabilization will be carried out on one of the outputs only, is determined. The procedure then sets the phase of the selected stabilization output using the value of U_{min}, measures the count rate and compares it with the previously measured minimum value. If the current value differs from the minimum by more than a certain fraction of the fringes amplitude (we use first a limit of 0.01, then 0.005 and finally 0.002), phase has drifted and has to be corrected. In order to correct the phase, the amount of phase drift has to be known. It can be calculated from the sine function behavior of the interference fringes, if a phase shift of $\pi/2$ is applied (using half of the value of half-wave voltage). A new U_{min} voltage value correcting for the phase drift which was found will then be calculated and

applied. The procedure will check again whether there is a minimum on the selected output and perform the phase correction again if the measured count rate has deviated from the minimum by more than the preset limit. In the case of two interferometers, the stabilization procedure is extended to comprise the possibility of stabilizing only the long or the short interferometer or both. The value of the variable "interf" indicates the first, the second or the third of the possibilities mentioned. The sketch of the main program for stabilization thus looks like:

```
if interf = 1 or interf = 2
    stabilize interferometer no. interf
else
    stabilize both interferometers simultaneously
end
```

In the case of simultaneous stabilization of the two interferometers, the following procedure is used to encompass the situation when one of the interferometers is stabilized before the other one:

```
while interferometer no.1 or interferometer no.2 are not stable
    if both are not stable
        stabilize both simultaneously
    end
        if interferometer no.1 (2) is not stable
        stabilize no.1 (2)
    end
end
```

If one of the interferometers is stabilized before the other one, the stabilization procedure will move on to the regime of single interferometer stabilization and the phase of the stabilized interferometer will be left to evolve according to the lab conditions. If the already stabilized interferometer will become unstable again, the procedure will return to the first part of the "while" cycle where both interferometers will be stabilized simultaneously or, alternatively, to the second part if the other interferometer has meanwhile been stabilized.

A maximum number of unsuccessful stabilization cycles is set, after which the stabilization procedure will try to make a few automatic corrections that could lead to successful stabilization: lower the visibility by ca. 5 standard deviations, measure interference fringes and calculate visibility

again and finally, scan the air gap in the unstable interferometer for better visibility. The number of available stabilization cycles will be increased after each of these steps to allow successful stabilization with new visibility values. If none of these corrections lead to successful stabilization, the stabilization procedure will be automatically aborted. The general process can be illustrated as follows (at the beginning of the procedure the maximum number of stabilization cycles is set to 5):

```
no. of cycles  = 0;
max.no. of stabilization cycles = 5;
lowering = 0;
    if no. of cycles  <  max.no. of stabilization cycles
        no. of cycles = no. of cycles + 1
        stabilize interferometers
    elseif no. of cycles = max.no. of stabilization cycles
        if lowering = 0
            lowering = 1;
        else
            error - automatic procedure was unsuccessful
        end
        visibility =  visibility - 5*std. of visibility
        max.no. of stabilization cycles = max.no. of stabilization cycles +5
        no. of cycles = no. of cycles + 1
        stabilize interferometers
    else
        measure fringes, calculate visibility
        if visibility < minimum required visibility
            scan the air gap
            if visibility < minimum required visibility
                error - automatic procedure was unsuccessful
            end
        end
        max.no. of stabilization cycles = max.no. of stabilization cycles +5
    end
```

where "stabilize interferometers" stands for procedures which were previously indicated as "stabilize both simultaneously" and "stabilize no.1 (2)" .The previous scheme is part of the "while" cycle described above, so every time all the conditions mentioned are checked, the program returns to the while condition.

In the formerly described case of nonsimultaneously stabilized interferometers, the number of stabilization cycles will be reset, if phase in one of the interferometers has become unstable sometime after a successful stabilization while the other is being stabilized, so that both can become stabilized simultaneously. This can be illustrated on the sketch shown above as follows:

```
while interferometer no.1 or interferometer no.2 are not stable
    if both are not stable
        no. of cycles = no. of cycles + 1
        stabilize both simultaneously
    end
    if interferometer no.1 (2) is not stable
        no. of cycles 1 (2) = no. of cycles
        no. of cycles = 0
        no. of cycles 1 (2) = no. of cycles 1 (2) + 1
        stabilize no.1 (2)
    end
end
```

8 Adjustment and final measurement

8.1 Adjustment with strong light signal from probe laser diode

1. Setting the polarization of the light beam that it is divided by the PBS 50:50. These beams are coupled into the fibres by input signal and idler coupling lenses (SCL, ICL), see Fig. 5.1.

2. Polarization optimalization of the coupled light in front of the input polarizers (SP, IP) using polarization controllers (SPC, IPC).

3. Checking the coupling efficiency of air gaps.

4. Monitoring the visibility on the oscilloscope - setting the losses in arms of both intefreromeeters and polarization overlap.

5. Scanning the air gap by the manual stage - finding the maximum visibility (then repeating the step above).

8.2 Adjustment with weak (quantum) signal

1. Preparation of counters - connection of QUAD, QUAD2, DUAL.

2. Attenuation of the probe laser diode - setting count rates ca. million photons per second.

3. Conection of the signal from source to the experiment - same as for strong signal.

4. Optimalization of photons polarization in front of the input polarizers.

5. Measurement of the dark counts and background, when the beam is blocked.

6. Measurement of the visibility.

7. Testing of the action of choppers and flippers.

8.3 Settings of coincidence logic

1. Conection of coincidence logic - preparation and setting the delay lines, see Fig. 8.2, 9.1.

2. Scanning air gaps by motorized stages and finding Hong-Ou-Mandel dips.

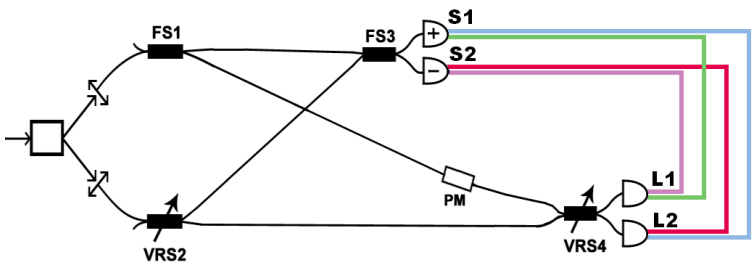

Figure 8.1: Scheme of the first coincidence measuement of the gate without feed-forward

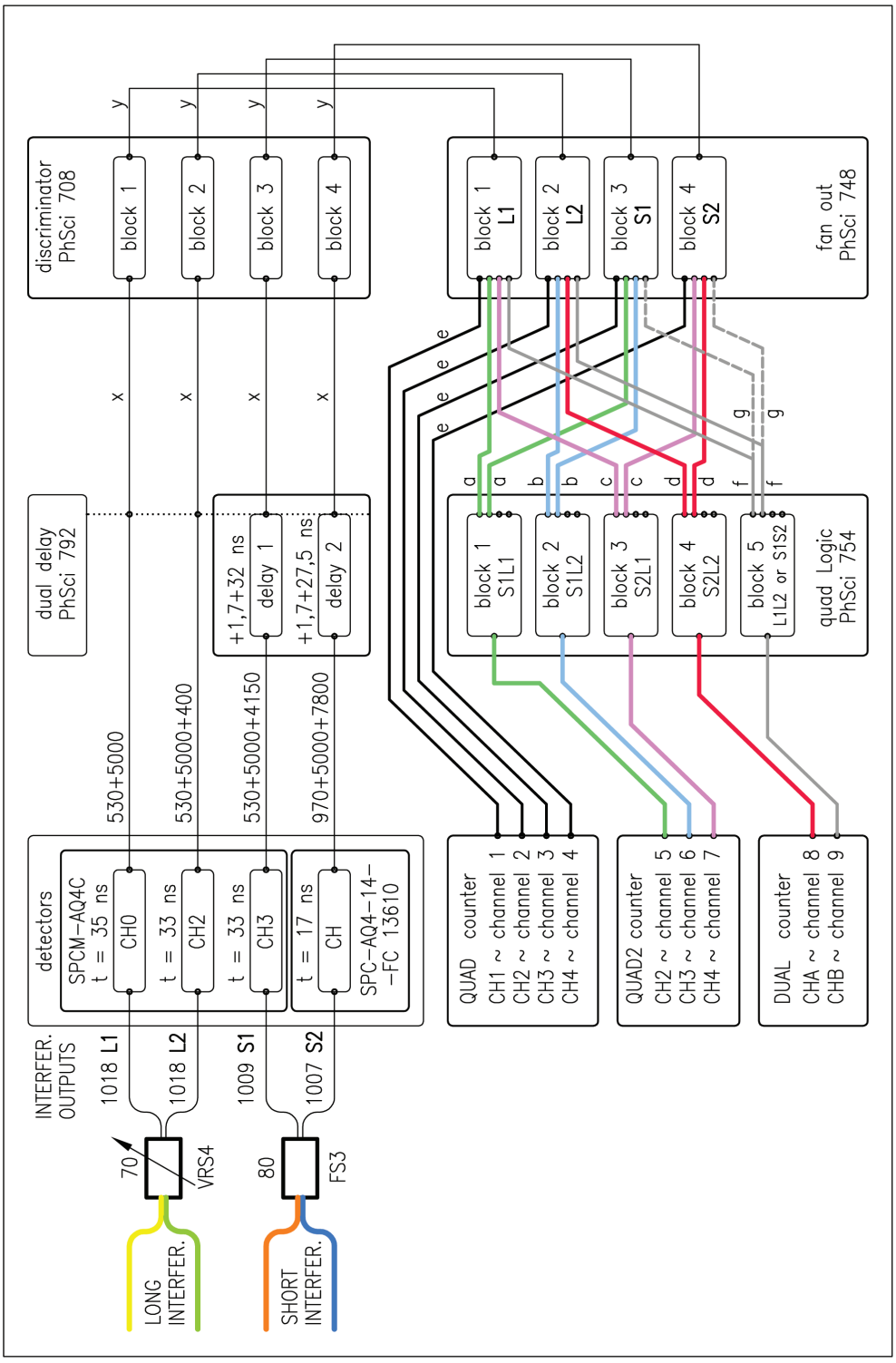

Figure 8.2: Scheme of timing and coincidence measurement

8.4 Final measurement

Structure of the main program in the case when all the fibre splitters have splitting ratio around 50:50

```
initialization:
    QUAD, QUAD2 with external time base
    DUAL, analog outputs, digital outputs
    set time base on DUAL - PROBE time (0.1s)
    - flippers passability test
    - choppers passability test, then block blue beam
    - measurrement of background
    - load of - relative efficiency of detectors
              - half-wave voltage
-------------------------------------------------
   measurement of visibilities (both interfetometers)
   for a:1:20 (how many measurement we want)
       stabalization of both interferometers

       change choppers - probe diode is blocked
       set time base on DUAL - PAIR time (3s)
       councidences measurement
       - save the data

       change choppers - pairs are blocked
       set time base on DUAL - PROBE time (0.1s)
   end
-------------------------------------------------
   set 0V to analog outputs
   close and clear everything
```

First we tested if the gate do its operation without feed-forward action. We measure coincidences as is shown on Fig. 8.1 Than we involved the feed-forward and we set the half-wave voltage of Green phase modulator. We tested the gate again in the same way as is shown on Fig. 8.3

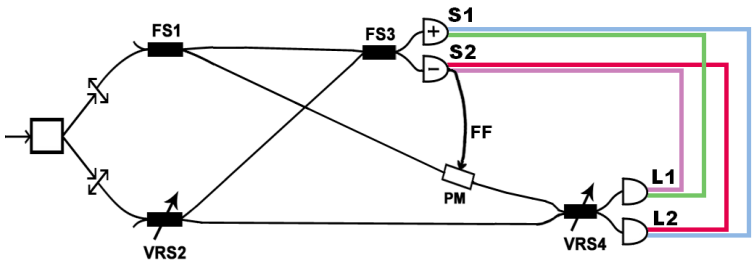

Figure 8.3: Scheme of the second coincidence measuement of the gate with feed-forward

8.5 Results

The results of the first coincidence measurement are summarized in upper part of Tab. 6. The numbers of coincidences corrected for the relative detection efficiency of detectors (Tab. 4) are in the middle part of the table. In the last part there are fidelities of the measured states.

As we expected the coincidences S1L1 and S1L2 are similar for both type of measurement - they correspond to the projection of program qubit state into basis state $|\varphi_+\rangle$. Coincidences S2L1 and S2L2 correspond to the projection of program qubit state into basis state $|\varphi_-\rangle$ and by the feed-forward the data qubit state is affected. We can see from the results that feed-forward is working properly and the succes probability of the gate is increased.

The fidelity of the data qubit state affected by the feed forward is 74% which is below the unity theoretical limit. The lower value of fidelity observed can be explained by imperfect interference of the photons at beam splitters FS3 and VRS4 because of their partial distinguishability. Particularly, the time of arrival was not aligned perfectly (it will require automatic scan of both Hong-Ou-Mandel dips). There is a small remaining difference in duration of photon wave packets due to slightly different dispersion in individual arms. Further, beam splitters FS3 and VRS4 deviates from ideal 50:50 by approximately 3.27% and 0.2%, respectively. Another significant source of errors is caused by imperfect setting of the voltage divider which generates a phase correction in Green arm different from the exact value of half-wave voltage of corresponding phase modulator Green S/N:75835. As the presented measurement is preliminary we expect improved fidelity in future.

Table 6: Table of measured coincidences per 3 s

nmeasured coincidences				
	S1L1	S1L2	S2L1	S2L2
without feed-forward	81	3	2	72
with feed-forward	76	3	52	18
normalized coincidences to detectoion efficiency				
without feed-forward	84	3	3	88
with feed-forward	79	3	64	22
fidelities [%]				
without feed-forward	97		97	
with feed-forward	96		74	

9 Conclusion

We have proposed the programmable phase gate and theoretically predicted its behaviour including losses and extra phase shifts. We have characterized all used components and successfully experimentally implemented the programmable phase gate using fibre components. Further, we have implemented programs for automatic control of the gate in MATLAB environment i.e. active simultaneous stabilization of both interferometers, automatic settings of splitting ratio of variable ratio splitter, and others. We have also prepared timing of entire experiment, coincidence measurement and especially the feed-forward loop. We have conducted the first test of the programmable phase gate without and with the feed-forward which increases the succes probabity of our gate.

All our programs and measurement procedures are implemented in MATLAB and included on the CD attached.

In the future, we want to fully characterize our programmable phase gate by quantum process tomography. Quantum tomography enables us to reconstruct both the density matrix of the output states and the Choi matrix of the process using maximum-likelihood method [8]. We will use already implemented software for full thomography measurement which includes programs for settings the splitting-ratios of variable ratio splitters, active stabilization of interferometers and other mentioned programs. The developed setup enables us to test other quantum theoretical predictions such as the minimal disturbance measurement. In future, we would like to fully exploit the advantages of stable path encoded quantum bits implementation and the promising technique of fast electronic feed-forward.

References:

[1] G. Vidal, L. Masanes and J. I. Cirac, *Storing quantum dynamics inquantum states: stochastic programmable gate for U*1 *operations*, Phys. Rev. Lett. **88**, 047905 (2002).

[2] M. Mičuda, M. Ježek, M. Dušek and J. Fiurášek, *Experimental realization of a programmable quantum gate*, Phys. Rev. A **78**, 062311 (2008).

[3] M. A. Nielsen and I. L. Chuang, *Programmable quantum gate arrays*, Phys. Rev. Lett. **79**, 321 (1997).

[4] T.B. Pittman, B.C Jacobs, and J.D. Franson *Demonstration of feed-forward control for linear optics quantum computation (Demonstration of Quantum Error Correction using Linear Optics)*, Phys. Rev. A **66**, 052305 (2002).

[5] M. Hendrych, M. Dušek, O. Haderka, *The effect of beam-splitter imperfections and losses on fringe visibility in a Mach-Zehnder interferometer*, Acta Physica Slovaka **46**, p. 393 (1996).

[6] P.W. Shor, in: *Proceedings of the 35th Annual ACM Symposium on the Foundation of Computer Science, Santa Fe, ed. S. Goldwasser*, (IEEE Computer Society, Los Alamitos, CA, 1994), s. 124.

[7] L. K. Grover, in: *Proceedings of the 28th Annual ACM Symposium on the Theory of Computing, Philadelphia*, (IEEE Computer Society, 1996), s. 212.

[8] M. Ježek, J. Fiurášek, and Z. Hradil, *Quantum inference of states and processes*, Physical Review A 68, 012305 (2003).

[9] G. G. Stokes, Cambridge & Dublin Mathematical Journal **4**, 1 (1849).

[10] L. Mandel, E. Wolf, *Optical Coherence and Quantum Optics*, Cambridge University Press, Cambridge, (1995).

[11] R. A. Campos, B. E. A. Saleh, M. C. Teich, Physical Review A **3**, 1371 (1989).

[12] H. Fikerová, Bachelor thesis: *Optical setups for quantum information processing*, Department of Optics, UP in Olomouc 2010.

[13] E. Halenková, Bachelor thesis: *Konstrukce vláknově optického interferometrického zařízení pro kvantově optické experimenty*, Department of Optics, UP in Olomouc 2008.

[14] I. Straka, private communication, Department of Optics, UP in Olomouc (10.4.2011).

[15] Bahaa E. A. Saleh, Malvin Carl Teich, *Fundaments of Photonics*, Wiley interscience - 2. edition, New Jersey 2007.

[16] Bahaa E. A. Saleh, Malvin Carl Teich, *Základy fotoniky*, matfyzpress, Praha 1994.

[17] M. Dušek, *Koncepční otázky kvantové teorie*, Department of Optics, UP in Olomouc 2002.

[18] L. Bartůšková, M. Dušek, J. Fiurášek, Z. Hradil, M. Ježek, M. Mičuda, L. Slodička, *Vláknová optika na telekomunikačních vlnových délkách*, report, Department of Optics, UP in Olomouc 2008.

[19] M. Dušek, protokol: *Měření půlvlnného napětí fázových modulátorů*, protocol on measurement, Department of Optics, UP in Olomouc (4.11.1997).

[20] M. Dušek, *Aktivní stabilizace interference*, report, Department of Optics, UP in Olomouc 1997.

[21] L. Bartůšková, *Měření doby odezvy SPCM*, protocol on measurement, Department of Optics, UP in Olomouc (17.6.2008).

[22] Canadian Instrumentation and reasearch, Ltd., *Model 905E Variable Ratio Coupler, Model 914-2 Piezo Controller*, datasheet (14.12.2005).

[23] Perkin Elmer Optoelectronics, *SPCM-AQ4C prototype (2) S/N:B4*, datasheet (9.9.2002) `http://www.scitecinstruments.pl/detektory/pcm/pdf/SPCMAQ4C.pdf`.

[24] Thorlabs, Motorized Filter Flipper (30.4.2011) `http://www.thorlabs.com/NewGroupPage9.cfm?ObjectGroup_ID=3962`.

[25] Thorlabs, Broadband Dielectric Mirrors (1.5.2011) `http://www.thorlabs.de/NewGroupPage9.cfm?ObjectGroup_ID=139&pn=BB1-E03`.

[26] Thorlabs, Molded Glass Aspheric Lenses (1.5.2011)
http://www.thorlabs.de/NewGroupPage9.cfm?ObjectGroup_ID=3811&pn=C220TME-B.

[27] Thorlabs, PIN photodiode (1.5.2011)
http://www.thorlabs.com/Thorcat/13000/13053-S01.pdf,
http://www.thorlabs.com/Thorcat/13000/13051-S01.pdf.

[28] LeCroy, WavePro 7 digital osciloskop (1.5.2011)
http://www.lecroy.com/files/pdf/LeCroy_WavePro_7_Zi-A_Datasheet.pdf.

[29] Single-Mode Fiber (2.5.2011)
http://www.nufern.com/specsheets/780hp.pdf.

Appendix

The time evolution of our experiment:

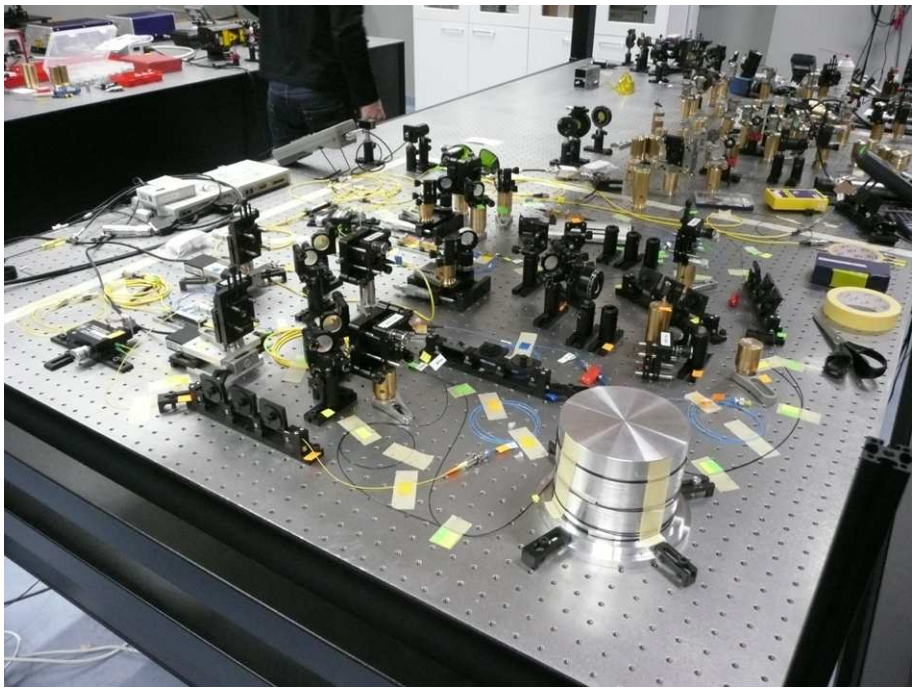

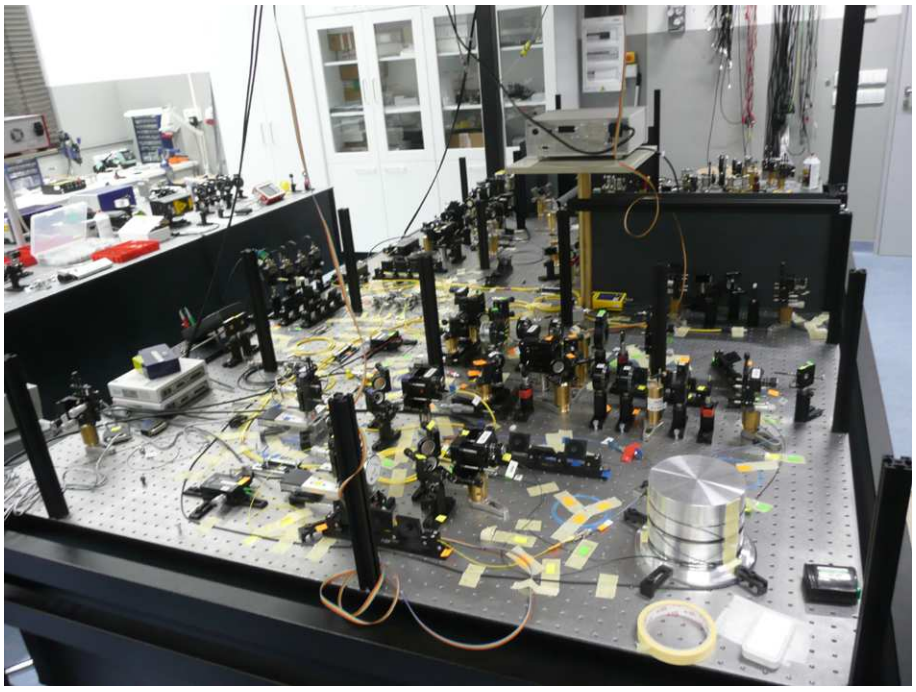

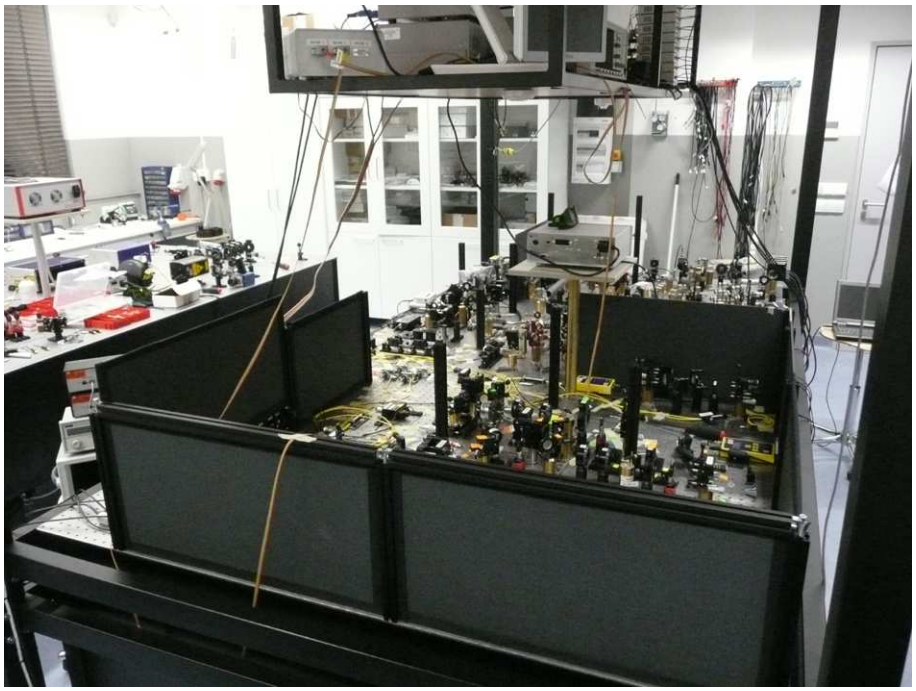

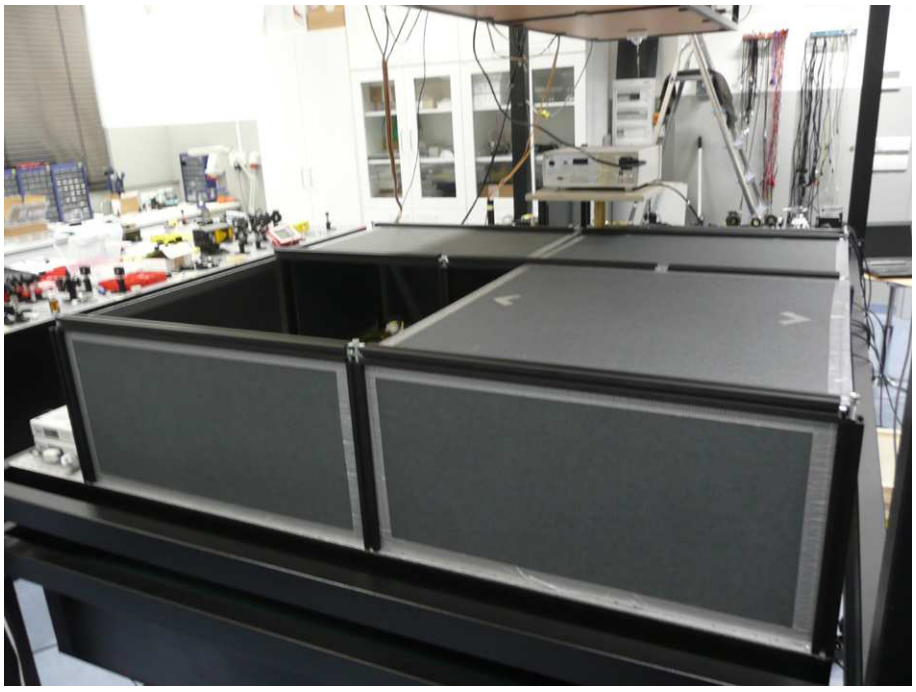

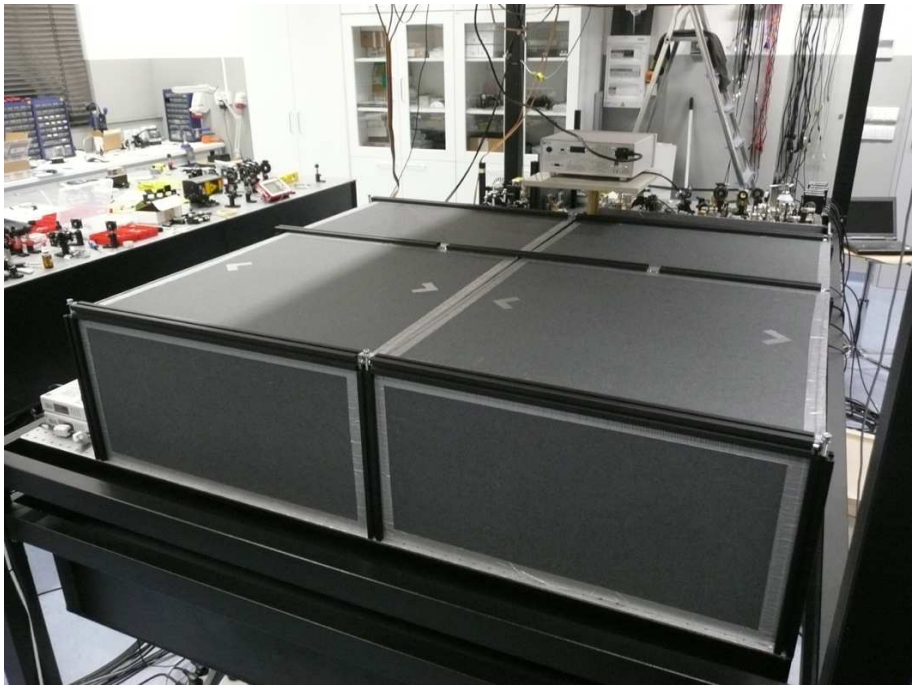

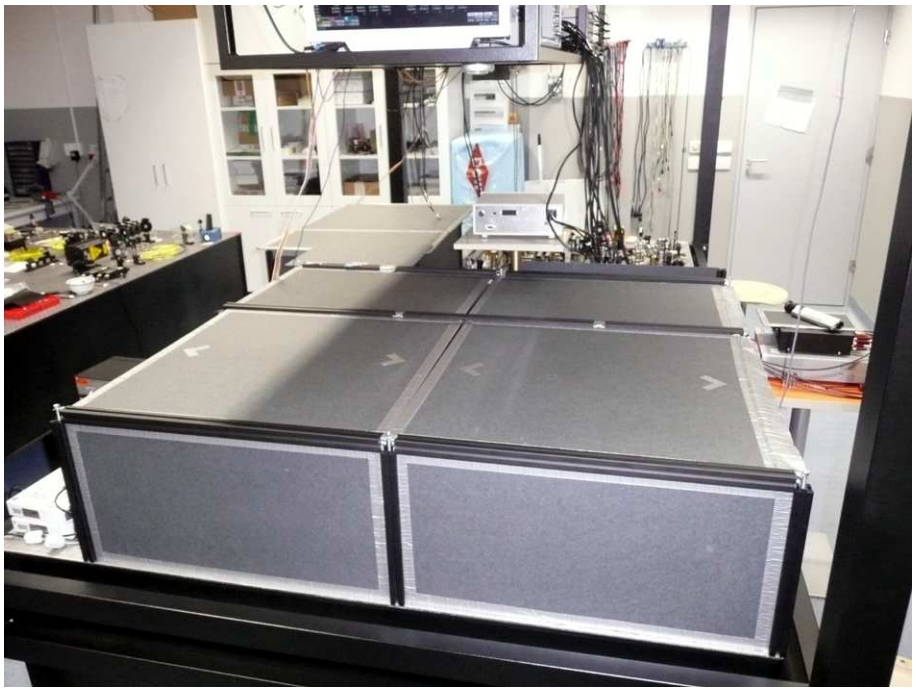

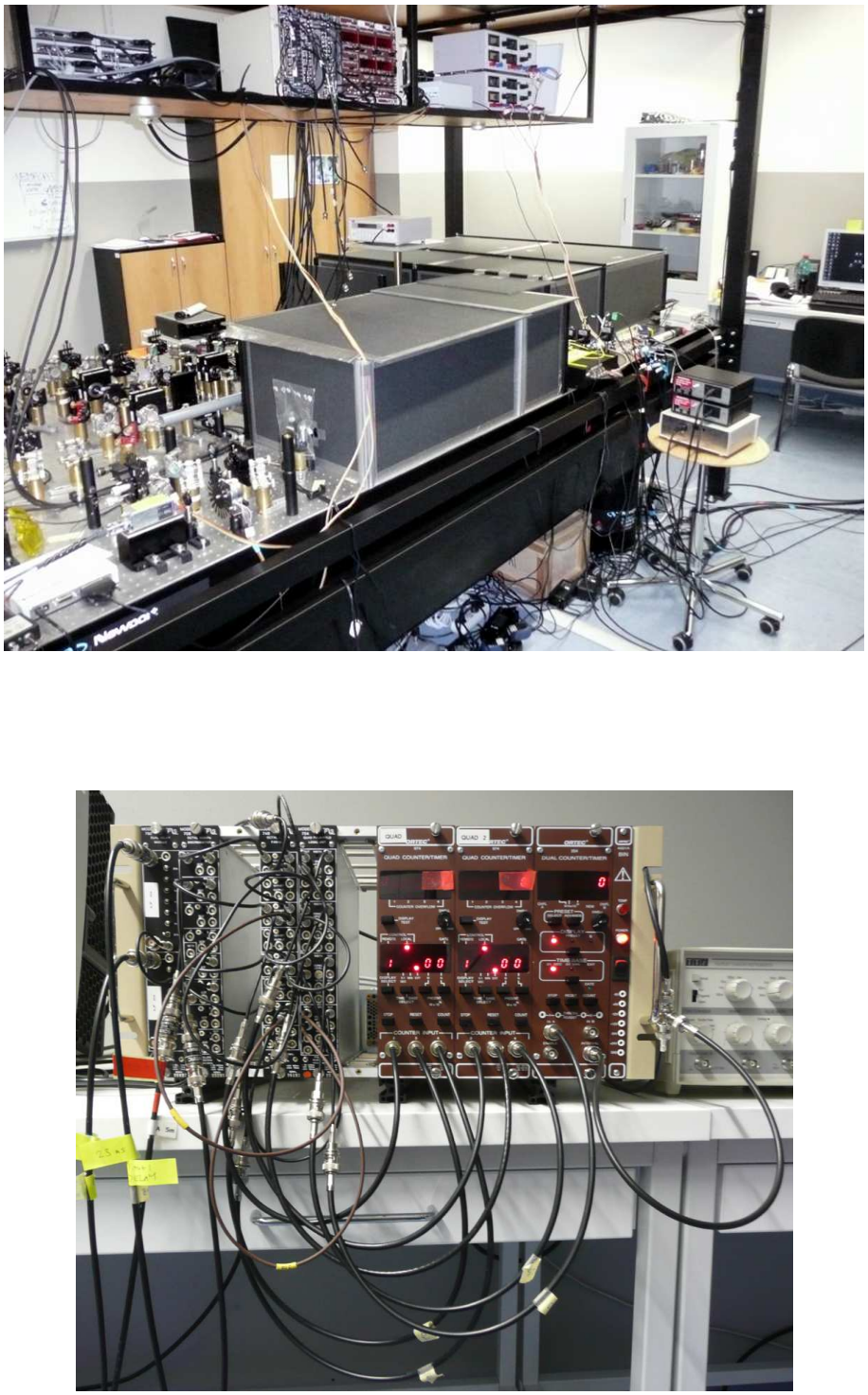

Figure 9.1: Photo coinsidence measurement